

Three-dimensional spatial normal modes in compressible boundary layers

ANATOLI TUMIN

Department of Aerospace and Mechanical Engineering, The University of Arizona,
Tucson, AZ 85721, USA

(Received 14 January 2006 and in revised form 17 April 2007)

Three-dimensional spatially growing perturbations in a two-dimensional compressible boundary layer are considered within the scope of linearized Navier–Stokes equations. The Cauchy problem is solved under the assumption of a finite growth rate of the disturbances. It is shown that the solution can be presented as an expansion into a biorthogonal eigenfunction system. The result can be used in a decomposition of flow fields derived from computational studies when pressure, temperature, and all the velocity components, together with some of their derivatives, are available. The method can also be used if partial data are available when *a priori* information may be utilized in the decomposition algorithm.

1. Introduction

The conventional linear stability theory of boundary layers deals with the quasi-parallel flow approximation when the characteristic scale of the perturbations, λ (wavelength), is much smaller than the longitudinal scale of the mean flow, L : i.e. $\lambda \ll L$. In this approximation, the solution of the linearized Navier–Stokes equations is considered in the form of normal modes

$$q(x, y, z, t) = \hat{q}(y) \exp(i(\alpha x + \beta z - \omega t)), \quad (1.1)$$

where x , y , and z are the Cartesian coordinates, and coordinate y stands for distance from the wall; t is the time; α and β are the x - and z -components of the wavenumber, respectively. The analysis can be carried out within the scope of the temporal or spatial approach.

In the case of temporal analysis, the wavenumber of the perturbation is considered as a real parameter and the complex frequency has to be determined. For incompressible boundary layer flow, Grosch & Salwen (1978) showed that there are normal modes of discrete and continuous spectra. Later, Salwen & Grosch (1981) proved that the solution of the initial-value problem (Gustavsson 1979) can be presented as an expansion in these normal modes. Their weights can be found from the initial data with the help of the eigenfunctions of the adjoint problem. There is an orthogonality condition between the eigenfunctions of the direct and adjoint problems, and the sets of eigenfunctions are called a biorthogonal eigenfunction system. Recently, this result was extended to the cases of two- (Fedorov & Tumin 2003) and three-dimensional (Forgoston & Tumin 2005) perturbations in compressible boundary layers.

In the case of a spatial framework, frequency is prescribed as a real parameter. For two-dimensional mean flow with coordinate x in the downstream direction, β is a

real parameter, and the complex wavenumber, α , has to be found. The corresponding biorthogonal eigenfunction system for spatially growing disturbances was introduced independently by Zhigulev, Sidorenko & Tumin (1980) and Salwen & Grosch (1981) for two-dimensional perturbations in incompressible boundary layers. In addition to discrete modes (Tollmien–Schlichting-type modes), there are four branches of continuous spectra. The modes of two branches have arbitrary large growth rates in the downstream direction (they may be interpreted as upstream decaying modes). This indicates that a spatial Cauchy problem is ill-posed. Tumin & Fedorov (1983*b*) suggested considering spatial initial-value problems having finite growth rates in the downstream direction. In the case of incompressible flow, the initial data require velocity and pressure perturbations, together with some derivatives with respect to x . The constraint on the initial data providing finite growth rates in the downstream direction means that the short-scale upstream perturbations are not included in the initial data. Under this condition, the Laplace transform with respect to x can be utilized. When additional *a priori* information is available, the spatial initial-value problem can be solved with partial inflow data. For example, Tumin (2003) illustrated by an example that when the downstream boundary is far away (on the length scale of the upstream perturbations) one can assume that the solution can be expanded into downstream modes only, and the spatial initial-value problem is solvable with only velocity perturbations as the initial data.

Apparently, recovering the whole flow field from one velocity component is impossible, even under the assumption that only downstream modes are involved in the solution. However, if it is known that the main input into the perturbations is associated with a finite number of specific modes, one can still find their amplitudes. For example, two unstable discrete modes coexist in a laminar wall jet. Therefore, Tumin *et al.* (1996) assumed that experimental data were composed of the unstable modes only and found their amplitudes and phases from experimental data for one velocity component only. Afterwards, the quality of the decomposition could be checked by comparing the experimental data with data obtained with the help of the utilized normal modes and their recovered weights. Guydos & Tumin (2004) illustrated this approach by an example of two-dimensional perturbations in a compressible boundary layer. One can see that decomposition of experimental data should depend on the quality of the assumptions. In compressible boundary layers, results of measurements could be contaminated by acoustic perturbations that can penetrate into the boundary layer. Therefore, in order to provide a reasonable accuracy of the decomposition aimed at a discrete mode, one also needs data for the external acoustic field (Guydos 2004).

An analysis of compressible (Tumin & Fedorov 1983*b*) and incompressible (Zhigulev & Tumin 1987) boundary layers using the Laplace transform with respect to the streaming coordinate, x , demonstrated the completeness of the biorthogonal eigenfunction system for two-dimensional perturbations. Three-dimensional spatially growing/decaying perturbations in an incompressible boundary layer were considered by Tumin (2003). A biorthogonal eigenfunction system for three-dimensional perturbations in compressible boundary layers was formally introduced by Tumin (1983) without analysis of the spatial initial-value problem, which is necessary to establish an expansion of the solution into normal modes of discrete and continuous spectra.

The biorthogonal eigenfunction system was found to be a powerful tool for solving receptivity problems for boundary layers and for internal flows (Zhigulev *et al.* 1980; Fedorov 1982; Tumin & Fedorov 1983*a*; Tumin 1983; Tumin & Fedorov 1984;

Fedorov 1984; Zhigulev & Fedorov 1987; Fedorov 1988; Hill 1995; Tumin 1996; Tumin & Aizatulin 1997; Tumin 1998; Fedorov & Khokhlov 2002; Fedorov 2003*a, b*). Originally, the method was utilized for analysis of discrete modes (Tollmien–Schlichting-type modes) only. After clarification of uncertainties associated with the continuous spectra (Tumin 2003), the method was also applied to the analysis of roughness-induced perturbations (Tumin & Reshotko 2004, 2005; Tumin 2006*b*). It was proven (Tumin & Aizatulin 1997; Tumin 2006*a*) that the receptivity solution based on the biorthogonal eigenfunction expansion is equivalent to the method used by Ashpis & Reshotko (1990), whereas in the triple-deck limit the method leads to the results by Smith, Sykes & Brighton (1977) and Terent'ev (1981).

Another emerging application of the biorthogonal eigenfunction system is associated with the progress being made in computational fluid dynamics (CFD), which provides an opportunity for reliable simulation of such complex phenomena as boundary layer receptivity and laminar–turbulent transition (Ma & Zhong 2001, 2003*a, b*, 2005; Zhong & Ma 2002; Egorov, Fedorov & Nechaev 2004; Egorov, Fedorov & Soudakov 2005; Wang & Zhong 2005, 2007). In addition to experimental observations, CFD provides complete information about the flow field that cannot be measured in real experiments. However, this increase in available information does not furnish physical insight to the problem because the leading mechanisms still remain hidden behind a messy disturbance field. Sometimes a flow possesses several discrete modes that are equally significant in the transition process, and it might be desirable to distinguish the dynamics of each mode in the complex non-steady flow field. Consequently, the problem of flow fields decomposing into normal modes arises. Guydos & Tumin (2004) demonstrated how the biorthogonal eigenfunction system could be applied to an analysis of CFD data for two-dimensional perturbations in a compressible boundary layer. In order to find the amplitudes of the normal modes comprising the perturbations, it is necessary to provide velocity components, temperature, pressure, and some of their derivatives at one cross-section only. The orthogonality relation for the eigenfunctions of the direct and adjoint problems provides a straightforward tool to filter out amplitudes of the modes. Tumin, Wang & Zhong (2007) applied the technique to analyse perturbations generated in a high-speed boundary layer by blowing–suction through a slot on the wall. Amplitudes of stable and unstable discrete modes were filtered out from the CFD results and compared with the solution of the receptivity problem. Their work illustrates how the biorthogonal eigenfunction system could be used to gain insight into the details of the flow field that would have remained hidden without the advanced analysis. Future progress of computational efforts will be associated with three-dimensional perturbations (Wang & Zhong 2007), and an extension of the multimode decomposition method is required.

The objective of the present paper is to solve the spatial initial-value problem for three-dimensional perturbations in a compressible boundary layer, and to decompose the solution into the normal modes of the discrete and continuous spectra.

Briefly, the structure of the paper is as follows. The spatial Cauchy problem is solved in §2. Section 3 provides a brief recapitulation of the continuous and discrete spectra in compressible boundary layers. In §4, the biorthogonal eigenfunction system is utilized to decompose three-dimensional perturbations into modes of discrete and continuous spectra. A discussion and summary of the results are given in §5. Appendix A contains non-zero elements of matrices that are introduced in the governing equations. In Appendix B, we present definitions and details relevant to the biorthogonal eigenfunction system for spatially growing/decaying three-dimensional perturbations. Details of the numerical methods are provided in Appendix C.

2. Spatial Cauchy problem

We consider a compressible two-dimensional boundary layer in Cartesian coordinates, where x and z are the downstream and spanwise coordinates, respectively, and coordinate y corresponds to the distance from the wall. We write the governing equations (the linearized Navier–Stokes equations) for a periodic-in-time perturbation, $\sim \exp(-i\omega t)$, in the matrix form

$$\frac{\partial}{\partial y} \left(\mathbf{L}_0 \frac{\partial \mathbf{A}}{\partial y} \right) + \mathbf{L}_1 \frac{\partial \mathbf{A}}{\partial y} = \mathbf{H}_1 \mathbf{A} + \mathbf{H}_2 \frac{\partial \mathbf{A}}{\partial x} + \mathbf{H}_3 \frac{\partial \mathbf{A}}{\partial z}, \quad (2.1)$$

where vector \mathbf{A} has 16 components:

$$\mathbf{A}(x, y, z) = (u, \partial u / \partial y, v, \pi, \theta, \partial \theta / \partial y, w, \partial w / \partial y, \partial u / \partial x, \partial v / \partial x, \partial \theta / \partial x, \partial w / \partial x, \partial u / \partial z, \partial v / \partial z, \partial \theta / \partial z, \partial w / \partial z)^T. \quad (2.2)$$

\mathbf{L}_0 , \mathbf{L}_1 , \mathbf{H}_1 , \mathbf{H}_2 , and \mathbf{H}_3 are 16×16 matrices (their definitions are given in Appendix A); u , v , w , π , and θ represent three velocity components, pressure, and temperature perturbations, respectively; and the superscript T in (2.2) and in what follows stands for the transpose. The mean flow is assumed to be parallel (quasi-parallel approximation). Solution of (2.1) is subject to the following boundary conditions:

$$y = 0: \quad u = v = w = \theta = 0, \quad (2.3)$$

$$y \rightarrow \infty: \quad |A_j| \rightarrow 0 \quad (j = 1, \dots, 16). \quad (2.4)$$

We consider the spatial Cauchy problem for (2.1) assuming that the initial data, $\mathbf{A}_0(y, z)$, at $x=0$ correspond to the solution having a finite growth rate in the downstream direction.

After applying the Fourier transform with respect to the coordinate z and the Laplace transform with respect to x ,

$$\mathbf{A}_{p\beta}(y) = \int_0^\infty e^{-px} \int_{-\infty}^\infty e^{-i\beta z} \mathbf{A}(x, y, z) dz dx, \quad (2.5)$$

we arrive at the following system of ordinary differential equations:

$$\frac{d}{dy} \left(\mathbf{L}_0 \frac{d\mathbf{A}_{p\beta}}{dy} \right) + \mathbf{L}_1 \frac{d\mathbf{A}_{p\beta}}{dy} - \mathbf{H}_1 \mathbf{A}_{p\beta} - p\mathbf{H}_2 \mathbf{A}_{p\beta} - i\beta \mathbf{A}_{p\beta} = -\mathbf{H}_2 \mathbf{A}_{0\beta}, \quad (2.6)$$

where

$$\mathbf{A}_{0\beta}(y) = \int_{-\infty}^\infty e^{-i\beta z} \mathbf{A}_0(y, z) dz. \quad (2.7)$$

The homogeneous part of (2.6) can be recast as an equation for vector \mathbf{z} composed of the first eight elements of vector $\mathbf{A}_{p\beta}$ as follows:

$$\frac{d\mathbf{z}}{dy} = \mathbf{H}_0 \mathbf{z}, \quad (2.8)$$

where \mathbf{H}_0 is an 8×8 matrix.

There are eight fundamental solutions, $\mathbf{z}_1, \dots, \mathbf{z}_8$, of the homogeneous system of equations (2.8). Outside the boundary layer ($y \rightarrow \infty$), \mathbf{H}_0 is a matrix of constant coefficients, and thus each fundamental solution has an exponential asymptotic behaviour $\sim \exp(\lambda_j y)$, where $\lambda_1, \dots, \lambda_8$ are determined from the characteristic equation

$$\det \|\mathbf{H}_0 - \lambda \mathbf{I}\| = 0, \quad (2.9)$$

that can be recast as follows:

$$(b_{11} - \lambda^2)^2 \times [(b_{22} - \lambda^2)(b_{33} - \lambda^2) - b_{23}b_{32}] = 0, \quad (2.10)$$

where

$$b_{11} = H_0^{21}, \quad (2.11a)$$

$$b_{22} = H_0^{42}H_0^{24} + H_0^{43}H_0^{34} + H_0^{46}H_0^{64} + H_0^{48}H_0^{84}, \quad (2.11b)$$

$$b_{23} = H_0^{42}H_0^{25} + H_0^{43}H_0^{35} + H_0^{46}H_0^{65} + H_0^{48}H_0^{85}, \quad (2.11c)$$

$$b_{32} = H_0^{64}, \quad b_{33} = H_0^{65}, \quad (2.11d)$$

with H_0^{ij} denoting the (i, j) element of matrix \mathbf{H}_0 . The roots of (2.10) are (we substitute $p = i\alpha$)

$$\lambda_{1,2}^2 = \lambda_{7,8}^2 = b_{11} = \alpha^2 + \beta^2 + i\text{Re}(\alpha - \omega), \quad (2.12)$$

$$\lambda_{3,4}^2 = (b_{22} + b_{33})/2 + \frac{1}{2}\sqrt{(b_{22} - b_{33})^2 + 4b_{23}b_{32}}, \quad (2.13)$$

$$\lambda_{5,6}^2 = (b_{22} + b_{33})/2 - \frac{1}{2}\sqrt{(b_{22} - b_{33})^2 + 4b_{23}b_{32}}. \quad (2.14)$$

The root branches are chosen to have $\text{Re}(\lambda_1, \lambda_3, \lambda_5, \lambda_7) < 0$, and we define a matrix of fundamental solutions,

$$\mathbf{m} = \|\mathbf{z}_1, \dots, \mathbf{z}_8\|. \quad (2.15)$$

We use a lower-case \mathbf{z} for vectors having 8 components, whereas vectors having 16 components will be denoted by a capital \mathbf{Z} . By the definition of the components in (2.2), one can find all the components of the fundamental solutions \mathbf{Z} if the fundamental solutions \mathbf{z} are known.

The non-homogeneous system given by (2.6) has a solution expressed in the form

$$\mathbf{A}_p = \mathbf{M}\mathbf{Q}(y) + \mathbf{G}, \quad (2.16)$$

where \mathbf{M} is the matrix of fundamental solutions composed of vectors \mathbf{Z}_j ($j = 1, \dots, 8$), and the vector of coefficients $\mathbf{Q}(y)$ has to be found. Vector $\mathbf{G}(y)$ is defined as follows:

$$\left. \begin{aligned} G_1 = \dots = G_8 = 0, \\ G_9 = -F_9; \dots, G_{16} = -F_{16}, \end{aligned} \right\} \quad (2.17)$$

where F_j are components of the vector $\mathbf{F}(y) = -(\mathbf{H}_2\mathbf{A}_{0\beta})$. After substituting (2.16) into (2.6), we arrive at the following system of equations for \mathbf{Q} :

$$\begin{aligned} 2\mathbf{L}_0 \frac{d\mathbf{M}}{dy} \frac{d\mathbf{Q}}{dy} + \mathbf{L}_0\mathbf{M} \frac{d^2\mathbf{Q}}{dy^2} + \frac{d\mathbf{L}_0}{dy} \mathbf{M} \frac{d\mathbf{Q}}{dy} + \mathbf{L}_1\mathbf{M} \frac{d\mathbf{Q}}{dy} \\ + \mathbf{L}_1 \frac{d\mathbf{G}}{dy} - \mathbf{H}_1\mathbf{G} - p\mathbf{H}_2\mathbf{G} - i\beta\mathbf{H}_3\mathbf{G} = \mathbf{F}. \end{aligned} \quad (2.18)$$

Let us consider the individual equations of (2.18). Denoting as z_{ij} the i th component of vector \mathbf{z}_j , Q_j the j th component of vector \mathbf{Q} , and F_j the j th component of vector \mathbf{F} , then the first, third, fifth, sixth, and seventh equations of (2.18) are, respectively,

$$z_{1j} \frac{dQ_j}{dy} = 0, \quad z_{3j} \frac{dQ_j}{dy} = F_3, \quad z_{5j} \frac{dQ_j}{dy} = 0, \quad (2.19a-c)$$

$$z_{6j} \frac{dQ_j}{dy} - pF_{11} = F_6, \quad z_{7j} \frac{dQ_j}{dy} = 0, \quad (2.19d, e)$$

where the index summation rule is imposed, and the explicit form of the matrix elements (see Appendix A) is taken into account. Using (2.19b), and the definitions $Z_{10j} = pz_{3j}$ and $Z_{14j} = i\beta z_{3j}$, the second and eighth equations of (2.18) are, respectively,

$$z_{2j} \frac{dQ_j}{dy} + (m+1) \frac{dG_{10}}{dy} + (m+1)pF_3 + pH_2^{29}F_9 - i\beta(m+1)F_{12} = F_2, \quad (2.20a)$$

$$z_{8j} \frac{dQ_j}{dy} + (m+1)i\beta F_3 + (m+1) \frac{dG_{14}}{dy} + pG_{12} = F_8. \quad (2.20b)$$

The fourth equation of (2.18) is recast as

$$L_0^{43} \frac{dz_{3j}}{dy} \frac{dQ_j}{dy} + \frac{d}{dy} \left(L_0^{43} z_{3j} \frac{dQ_j}{dy} \right) + z_{4j} \frac{dQ_j}{dy} - pH_2^{4,10} G_{10} = F_4. \quad (2.21)$$

The third equation of (2.8) yields

$$\frac{dz_{3j}}{dy} = H_0^{31} z_{1j} + H_0^{33} z_{3j} + H_0^{34} z_{4j} + H_0^{35} z_{5j} + H_0^{37} z_{7j}. \quad (2.22)$$

After substitution of (2.22) into (2.21) and taking into account (2.19), we arrive at

$$z_{4j} \frac{dQ_j}{dy} = \left[F_4 - L_0^{43} H_0^{33} F_3 - \frac{d(L_0^{43} F_3)}{dy} + pH_2^{4,10} G_{10} \right] (1 + L_0^{43} H_0^{34})^{-1}. \quad (2.23)$$

Therefore, we have the following algebraic system of equations for dQ_j/dy :

$$m \frac{dQ}{dy} = \varphi, \quad (2.24)$$

where vector φ has the following eight components:

$$\varphi_1 = 0, \quad (2.25a)$$

$$\varphi_2 = F_2 - (m+1) \frac{dG_{10}}{dy} - (m+1)pF_3 - pH_2^{29}F_9 + i\beta(m+1)F_{12}, \quad (2.25b)$$

$$\varphi_3 = F_3, \quad (2.25c)$$

$$\varphi_4 = \left[F_4 - L_0^{43} H_0^{33} F_3 - \frac{d(L_0^{43} F_3)}{dy} + pH_2^{4,10} G_{10} \right] (1 + L_0^{43} H_0^{34})^{-1}, \quad (2.25d)$$

$$\varphi_5 = 0, \quad \varphi_6 = F_6 + pF_{11}, \quad \varphi_7 = 0, \quad (2.25e-g)$$

$$\varphi_8 = F_8 - (m+1)i\beta F_3 - (m+1) \frac{dG_{14}}{dy} - pG_{12}. \quad (2.25h)$$

One can solve the algebraic equations (2.24) and write the solution of (2.6) for the first eight components as follows:

$$A_{p\beta} = \sum_{j=1}^8 \left(a_j + \int_{y_j}^y \frac{dQ_j}{dy} dy \right) z_j, \quad (2.26)$$

where the constants a_j and y_j are determined using the boundary conditions. Using properties of determinants, we obtain the following solution:

$$\begin{aligned} \mathbf{A}_{p\beta} = & \left(a_1 + \int_0^{y_1} \frac{dQ_1}{dy} dy \right) \mathbf{z}_1 + \int_{\infty}^{y_2} \frac{dQ_2}{dy} dy \mathbf{z}_2 + \left(a_3 + \int_0^{y_3} \frac{dQ_3}{dy} dy \right) \mathbf{z}_3 + \int_{\infty}^{y_4} \frac{dQ_4}{dy} dy \mathbf{z}_4 \\ & + \left(a_5 + \int_0^{y_5} \frac{dQ_5}{dy} dy \right) \mathbf{z}_5 + \int_{\infty}^{y_6} \frac{dQ_6}{dy} dy \mathbf{z}_6 + \left(a_7 + \int_0^{y_7} \frac{dQ_7}{dy} dy \right) \mathbf{z}_7 + \int_{\infty}^{y_8} \frac{dQ_8}{dy} dy \mathbf{z}_8, \end{aligned} \tag{2.27}$$

where

$$\begin{aligned} a_1 &= \frac{c_2 E_{2357} + c_4 E_{4357} + c_6 E_{6357} + c_8 E_{8357}}{E_{1357}}, \\ a_3 &= \frac{c_2 E_{1257} + c_4 E_{1457} + c_6 E_{1657} + c_8 E_{1857}}{E_{1357}}, \\ a_5 &= \frac{c_2 E_{1327} + c_4 E_{1347} + c_6 E_{1367} + c_8 E_{1387}}{E_{1357}}, \\ a_7 &= \frac{c_2 E_{1352} + c_4 E_{1354} + c_6 E_{1356} + c_8 E_{1358}}{E_{1357}}, \\ c_j &= \int_0^{\infty} \frac{dQ_j}{dy} dy, \\ E_{ijkl} &= \det \begin{vmatrix} z_{1i} & z_{1j} & z_{1k} & z_{1l} \\ z_{3i} & z_{3j} & z_{3k} & z_{3l} \\ z_{5i} & z_{5j} & z_{5k} & z_{5l} \\ z_{7i} & z_{7j} & z_{7k} & z_{7l} \end{vmatrix}_{y=0}. \end{aligned}$$

Although the result (2.27) formally looks the same as in Forgoston & Tumin (2005), the derivatives dQ_j/dy are found from a different set of algebraic equations.

The inverse Laplace transform,

$$\mathbf{A}_{\beta}(x, y; \beta) = \frac{1}{2\pi i} \int_{p_0 - i\infty}^{p_0 + i\infty} \mathbf{A}_{p\beta}(y; p, \beta) e^{px} dp, \tag{2.28}$$

will be determined by the poles corresponding to the roots $E_{1357} = 0$, and by the branch cuts associated with the equations $\text{Re}(\lambda_1, \lambda_3, \lambda_5, \lambda_7) = 0$. The structure of the branch cuts is the same as in the case of two-dimensional perturbations (Guydos & Tumin 2004). They represent perturbations of the continuous spectra: vorticity, entropy, and acoustic modes. A brief recapitulation of the continuous spectra is provided in §3. The constraint on the initial data ensures that there is p_0 such that the solution is analytic at $\text{Re}(p) \geq p_0$ and the path of integration in (2.28) lies in the domain of analyticity of $\mathbf{A}_{p\beta}$.

The result (2.28) is recast as a sum of integrals along the sides γ^+ and γ^- of each left-hand-side branch in the complex plane p that represent input from the continuous spectra, and a sum of the residue values corresponding to the input from the discrete spectrum,

$$\mathbf{A}_{\beta} = -\frac{1}{2\pi i} \sum_m \left(\int_{\gamma_m^+} \mathbf{A}_{p\beta} e^{px} dp + \int_{\gamma_m^-} \mathbf{A}_{p\beta} e^{px} dp \right) + \sum_n \text{Res}_n(\mathbf{A}_{p\beta} e^{px}). \tag{2.29}$$

The three-dimensional character of the perturbations leads to overlapping of the two branches corresponding to the vorticity modes, similar to the cases of spatial

(Tumin 2003) and temporal (Forgoston & Tumin 2005) analysis of three-dimensional perturbations. The latter is reflected by the double root in (2.12).

In principle, the assumption of a finite growth rate of the solution (2.29) allows inclusion of a portion from the upstream modes into the initial data (Tumin & Fedorov 1983*b*; Tumin 2003). However, the typical applications of the method are associated with downstream modes only, and the upstream modes are excluded from the consideration.

Similar to the analysis of the initial-value problem, the integrals along the branch cut sides can be written as one integral of the difference $\mathbf{A}_{p\beta}^+ - \mathbf{A}_{p\beta}^-$, where superscripts + and - indicate values evaluated at sides γ^+ and γ^- , respectively. Although the coefficients c_j in (2.27) are different from those defined in Forgoston & Tumin (2005), all formulae for $\mathbf{A}_{p\beta}^+ - \mathbf{A}_{p\beta}^-$ remain the same for the spatial Cauchy problem under consideration. Particularly, for branch cuts corresponding to the acoustic waves, $\lambda_{3,4} = \pm ik$, where $k > 0$, we find

$$\begin{aligned} \mathbf{A}_{c,4} &= \mathbf{A}_{p\beta}^+ - \mathbf{A}_{p\beta}^- \\ &= \left(\frac{c_2 E_{1275}}{E_{1753} E_{1754}} + \frac{c_3 E_{1753}}{E_{1753} E_{1754}} + \frac{c_4 E_{1754}}{E_{1753} E_{1754}} + \frac{c_6 E_{1756}}{E_{1753} E_{1754}} + \frac{c_8 E_{7185}}{E_{1753} E_{1754}} \right) \\ &\quad \times (E_{5734} \mathbf{z}_1 + E_{1754} \mathbf{z}_3 + E_{7153} \mathbf{z}_4 + E_{7134} \mathbf{z}_5 + E_{1534} \mathbf{z}_7). \end{aligned} \quad (2.30)$$

All functions on the right-hand side (2.30) are evaluated at the γ^+ side of the branch cut, where $\mathbf{z}_3 \sim \exp(+iky)$.

In the region of overlapping vorticity modes, we can use the result for the initial-value problem to represent $\mathbf{A}_{p\beta}^+ - \mathbf{A}_{p\beta}^-$ as a sum of stand-alone modes corresponding to $\lambda_{1,2} = \lambda_{7,8} = \pm ik$ ($k > 0$):

$$\mathbf{A}_{p\beta}^+ - \mathbf{A}_{p\beta}^- = \mathbf{A}_{c,1} + \mathbf{A}_{c,5}, \quad (2.31)$$

where

$$\begin{aligned} \mathbf{A}_{c,1} &= \left(\frac{c_1 E_{1753}}{E_{1753} E_{2753}} + \frac{c_2 E_{2753}}{E_{1753} E_{2753}} + \frac{c_4 E_{4753}}{E_{1753} E_{2753}} + \frac{c_6 E_{6753}}{E_{1753} E_{2753}} + \frac{c_8 E_{8753}}{E_{1753} E_{2753}} \right) \\ &\quad \times (E_{2753} \mathbf{z}_1 - E_{1753} \mathbf{z}_2 + E_{1275} \mathbf{z}_3 + E_{1723} \mathbf{z}_5 + E_{1253} \mathbf{z}_7) \end{aligned} \quad (2.32)$$

and

$$\begin{aligned} \mathbf{A}_{c,5} &= \left(\frac{c_1 E_{1253}}{E_{2753} E_{2853}} + \frac{c_4 E_{5234}}{E_{2753} E_{2853}} + \frac{c_6 E_{2563}}{E_{2753} E_{2853}} + \frac{c_7 E_{7253}}{E_{2753} E_{2853}} + \frac{c_8 E_{8253}}{E_{2753} E_{2853}} \right) \\ &\quad \times (E_{7853} \mathbf{z}_2 + E_{2785} \mathbf{z}_3 - E_{2783} \mathbf{z}_5 - E_{2853} \mathbf{z}_7 + E_{2753} \mathbf{z}_8). \end{aligned} \quad (2.33)$$

We call modes (2.32) and (2.33) vorticity modes A and B, respectively. Here notation γ^+ corresponds to the branch-cut side where \mathbf{z}_1 and \mathbf{z}_7 have asymptotics $\sim \exp(+iky)$.

In the case of steady supersonic perturbations, there is an overlapping of two vorticity modes and the entropy mode with $\lambda_{5,6} = \pm ik$ ($k > 0$). For this case, we can also use the result for the initial-value problem,

$$\mathbf{A}_{p\beta}^+ - \mathbf{A}_{p\beta}^- = \mathbf{A}_{c,1} + \mathbf{A}_{c,2} + \mathbf{A}_{c,5}, \quad (2.34)$$

where $\mathbf{A}_{c,1}$ and $\mathbf{A}_{c,5}$ are given by (2.32) and (2.33), and

$$\begin{aligned} \mathbf{A}_{c,2} &= \left(\frac{c_1 E_{1283}}{E_{2853} E_{2863}} - \frac{c_4 E_{2834}}{E_{2853} E_{2863}} + \frac{c_5 E_{2853}}{E_{2853} E_{2863}} + \frac{c_6 E_{2863}}{E_{2853} E_{2863}} - \frac{c_7 E_{2783}}{E_{2853} E_{2863}} \right) \\ &\quad \times (E_{8563} \mathbf{z}_2 + E_{2856} \mathbf{z}_3 + E_{2863} \mathbf{z}_5 - E_{2853} \mathbf{z}_6 - E_{2563} \mathbf{z}_8). \end{aligned} \quad (2.35)$$

In (2.35), the side γ^+ also means that $\mathbf{z}_5 \sim \exp(+iky)$.

In the case of steady subsonic perturbations, there is an overlapping of four modes. This case has not yet been considered elsewhere. Similarly to the other cases, one can derive

$$\mathbf{A}_{p\beta}^+ - \mathbf{A}_{p\beta}^- = \mathbf{A}_{c,1} + \mathbf{A}_{c,2} + \mathbf{A}_{c,3} + \mathbf{A}_{c,5}, \quad (2.36)$$

where $\mathbf{A}_{c,3}$ is defined as follows:

$$\begin{aligned} \mathbf{A}_{c,3} = & \left(\frac{c_1 E_{6218}}{E_{2863} E_{2468}} - \frac{c_3 E_{2863}}{E_{2863} E_{2468}} + \frac{c_4 E_{2468}}{E_{2863} E_{2468}} - \frac{c_5 E_{6528}}{E_{2863} E_{2468}} - \frac{c_7 E_{6728}}{E_{2863} E_{2468}} \right) \\ & \times (E_{6348} \mathbf{z}_2 - E_{2468} \mathbf{z}_3 - E_{2863} \mathbf{z}_4 - E_{2834} \mathbf{z}_6 + E_{2463} \mathbf{z}_8). \end{aligned} \quad (2.37)$$

In addition, we should address the discrete spectrum, which is associated with poles originating from zeros, p_n , of the equation $E_{1357}(p_n) = 0$. Their input into (2.29) is presented by the residue values

$$\begin{aligned} \text{Res}_n(\mathbf{A}_p e^{p_n x}) = & \frac{e^{p_n x}}{(\partial E_{1357}/\partial p)} [\mathbf{z}_1 (c_2 E_{2357} + c_4 E_{4357} + c_6 E_{6357} + c_8 E_{8357}) \\ & + \mathbf{z}_3 (c_2 E_{1257} + c_4 E_{1457} + c_6 E_{1657} + c_8 E_{1857}) \\ & + \mathbf{z}_5 (c_2 E_{1327} + c_4 E_{1347} + c_6 E_{1367} + c_8 E_{1387}) \\ & + \mathbf{z}_7 (c_2 E_{1352} + c_4 E_{1354} + c_6 E_{1356} + c_8 E_{1358})], \end{aligned} \quad (2.38)$$

where the right-hand side is evaluated at $p = p_n$. Taking into account that $E_{1357} = 0$, one can derive from (2.38)

$$\begin{aligned} \text{Res}_n(\mathbf{A}_p e^{p_n x}) = & e^{p_n x} \frac{(c_2 E_{1257} + c_4 E_{1457} + c_6 E_{1765} + c_8 E_{1578})}{(\partial E_{1357}/\partial p) E_{1457}} \\ & \times (\mathbf{z}_1 E_{4357} + \mathbf{z}_3 E_{1457} + \mathbf{z}_5 E_{1347} + \mathbf{z}_7 E_{1354}). \end{aligned} \quad (2.39)$$

The result (2.39) represents a discrete mode that is composed of four fundamental solutions, \mathbf{z}_1 , \mathbf{z}_3 , \mathbf{z}_5 , and \mathbf{z}_7 , decaying outside the boundary layer. This result and the results for the continuous spectra were verified using *Mathematica* (Wolfram 1999).

One can see that input into the inverse Laplace transform (2.29) from the integrals along branch cuts [(2.30), (2.32), (2.33), (2.35), (2.37)], and the residue values evaluated at the poles (2.39) are written as stand-alone modes (vector functions) with coefficients depending on the initial conditions $\mathbf{A}_0(y, z)$,

$$\mathbf{A}_\beta(x, y) = \sum_\nu d_\nu \mathbf{A}_{\alpha_\nu}(y) e^{i\alpha_\nu x} + \sum_j \int_0^\infty d_j(k) \mathbf{A}_{\alpha_j}(y) e^{i\alpha_j(k)x} dk. \quad (2.40)$$

Here, \sum_ν and \sum_j denote sums over the discrete spectra and branches of the continuous spectra, respectively. The coefficients d_ν and d_j also can be found from the initial data, $\mathbf{A}_0(y, z)$, using the biorthogonal eigenfunction system $\{\mathbf{A}_{\alpha\beta}, \mathbf{B}_{\alpha\beta}\}$ defined in Appendix B. The solution (2.40) provides the background for the multimode decomposition that is discussed in §4.

3. Recapitulation of properties of spectra

3.1. Continuous spectra

Although one can find properties of continuous spectra for perturbations in compressible boundary layers elsewhere (Tumin & Fedorov 1983*b*; Balakumar & Malik 1992; Guydos & Tumin 2004), for the sake of clarity we briefly recapitulate these properties.

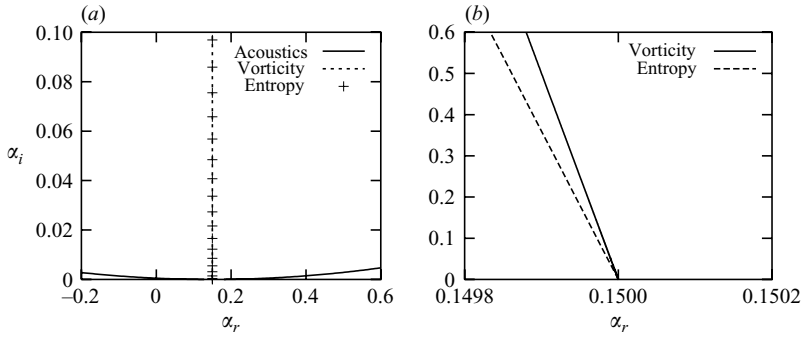


FIGURE 1. Branch cuts in the upper half-plane, α . $M = 5.95$, $F = 10^{-4}$, $Re = 1500$, $\beta = 10^{-4}$.

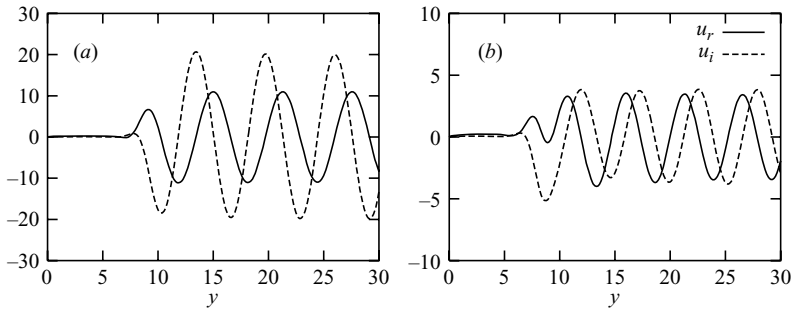


FIGURE 2. Streamwise velocity perturbation of (a) vorticity mode A and (b) entropy mode. $M = 5.95$, $T_w/T_{ad} = 0.1$, $F = 10^{-4}$, $Re = 1500$, $\beta = 0.16$, $k = 1$.

The structure of the three-dimensional continuous spectra is similar to the two-dimensional case discussed in Guydos & Tumin (2004). As in the two-dimensional case, there are seven branches. Three-dimensionality leads to two vorticity modes, A and B (see §2), stemming from the vector character of the quantity. There are branches associated with the upstream modes that are of no interest to the present work. Figure 1(a) shows branches of the downstream modes in the complex plane $\alpha = -ip$ (p is the Laplace variable in §2) at Mach number $M = 5.95$, Reynolds number $Re = 1500$, $\beta = 10^{-4}$, and frequency parameter $F = \omega\mu_e/\rho_e U_e^2 = 10^{-4}$, where the subscript e stands for the flow parameters at the edge of the boundary layer. In what follows, we use the specific heat ratio $\gamma = 1.4$, and assume that viscosity is a function of the temperature in accordance with Sutherland's law. Results in figure 1 were obtained at Prandtl number $Pr = 0.72$, free-stream stagnation temperature $T_0 = 470$ K, and bulk viscosity parameter $e = 0.8$ (see Appendix A). One can see two horizontal branches representing the slow (SA) and fast (FA) acoustic waves. In the limit of high Reynolds numbers, the branch points correspond to phase velocities $c = 1 \pm 1/M$. The vorticity and entropy modes are indistinguishable in the scale of figure 1(a), but they are not identical, as one can see from figure 1(b). However, there is an overlapping of the modes at $\omega = 0$. In the limit of high Reynolds numbers, the branch points of the vorticity and entropy modes are $\alpha \approx \omega$. One can find more details about the branch points for three-dimensional perturbations in Balakumar & Malik (1992).

In the case of three-dimensional perturbations, the modes of continuous spectra are composed of five fundamental solutions. Some of them are oscillating outside the boundary layer as $\sim \exp(\pm iky)$, whereas the others are decaying. Figures 2(a, b)

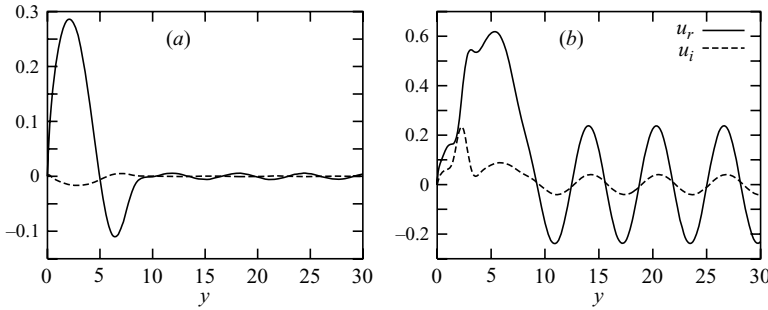


FIGURE 3. Streamwise velocity perturbation of (a) the fast and (b) slow acoustic modes. $M = 5.95$, $T_w/T_{ad} = 0.1$, $F = 10^{-4}$, $Re = 1500$, $\beta = 0.16$, $k = 1$.

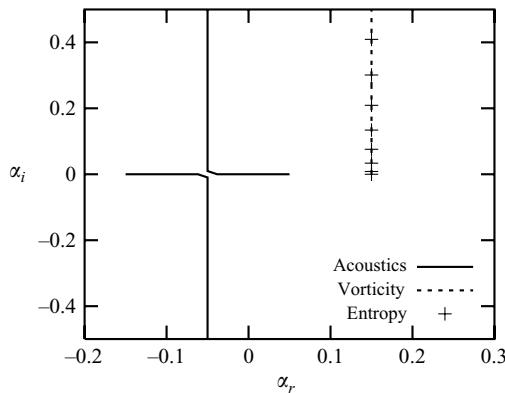


FIGURE 4. Branch cuts at $M = 0.5$, $F = 10^{-4}$, $Re = 1500$, $\beta = 10^{-4}$.

and 3(a,b) show real, u_r , and imaginary, u_i , parts of the streamwise velocity perturbations of the vorticity, entropy and two acoustic modes in the case of a boundary layer over a flat plate with temperature factor $T_w/T_{ad} = 0.1$, where T_w and T_{ad} are the wall temperature and the temperature of the adiabatic wall, respectively. We use the length scale $H = (\mu_e x / \rho_e U_e)^{1/2}$, where x is the distance from the leading edge. The continuous spectrum parameter in these examples is $k = 1$. The other parameters are the same as in figure 1, except the spanwise wavenumber, which is $\beta = 0.16$. The solutions are normalized by the wall condition $du/dy(0) = 1$. One can see that the vorticity and entropy modes do not penetrate the boundary layer at these parameters, whereas the acoustic modes have velocity perturbations significantly larger than outside the boundary layer. This phenomenon is the reason why the quality of perturbation measurements in high-speed boundary layers depends on the level of the acoustic perturbations originated in boundary layers over wind-tunnel walls.

Figure 4 shows branches of the continuous spectra in the complex plane, α , for a subsonic boundary layer at Mach number $M = 0.5$, $Re = 1500$, $F = 10^{-4}$, and $\beta = 10^{-4}$. In the limit $M \rightarrow 0$, the branch cuts corresponding to the acoustic modes degenerate to the imaginary axis of α . In the limit $Re \rightarrow \infty$, the acoustic branch cuts form a cross with the midpoint at $\alpha = -M^2\omega/(1 - M^2)$ (Fedorov 1982; Zhigulev & Tumin 1987).

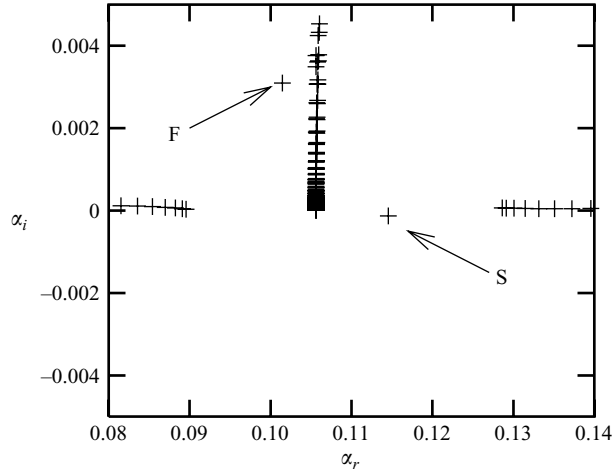


FIGURE 5. Eigenvalue map. $M = 5.6$, $F = 150 \times 10^{-6}$, $Re = 704$, $\beta = 5.77 \times 10^{-5}$.

3.2. Slow and fast discrete modes

As was found by Mack (1969), the discrete spectrum of perturbations in supersonic boundary layers is more complicated than in the subsonic case. Fedorov & Khokhlov (2001) noticed that at high Mach numbers (when the so-called second Mack's mode exists) there are two discrete modes (stable and unstable) that could be synchronized at some downstream coordinate, x , depending on the flow parameters and the perturbation frequency. Because at small Reynolds numbers one discrete mode is synchronized with the slow acoustic mode, whereas the other mode is synchronized with the fast acoustic mode, Fedorov (2003a) suggested calling them slow and fast discrete modes, respectively. The synchronization means that these discrete modes could be generated by acoustic waves interacting with the leading edge of a flat plate.

Both the slow and fast discrete modes could be involved in the laminar–turbulent transition scenario. For example, the decaying mode could be generated by the entropy or vorticity modes of the continuous spectra. At the point of synchronism between the fast and slow modes, the decaying mode can give rise to the unstable mode (switching of the modes), which may lead to the transition. The scenario suggested by Fedorov & Khokhlov (2001) means that both the stable and unstable modes are of interest for understanding transition mechanisms. Later, switching of the modes was observed in direct numerical simulations of perturbations in high-speed boundary layers (Ma & Zhong 2003b).

In order to clarify the terminology and to illustrate the motivation for analysis of stable discrete modes, we provide an example of slow and fast discrete modes in a boundary layer of a calorically perfect gas over a flat plate. The free-stream stagnation temperature $T_0 = 470$ K, the edge Mach number $M = 5.6$, the Prandtl number $Pr = 0.71$, and we employ Stokes' hypothesis ($e = 0$ in the matrix elements of Appendix A).

In the limit of two-dimensional perturbations, we choose a small spanwise wave-number, $\beta = 5.7 \times 10^{-5}$. The local Reynolds number, $Re = 704$. Figure 5 shows the map of eigenvalues obtained with the help of the spectral collocation method. The frequency parameter is $F = 150 \times 10^{-6}$. One can see the discretized continuous spectra. There are two horizontal branches corresponding to the slow and fast acoustic modes, and a vertical branch corresponding to the vorticity and entropy modes. Also, one can see fast (F) and slow (S) discrete modes. Figure 6(a, b) illustrates real, α_r , and

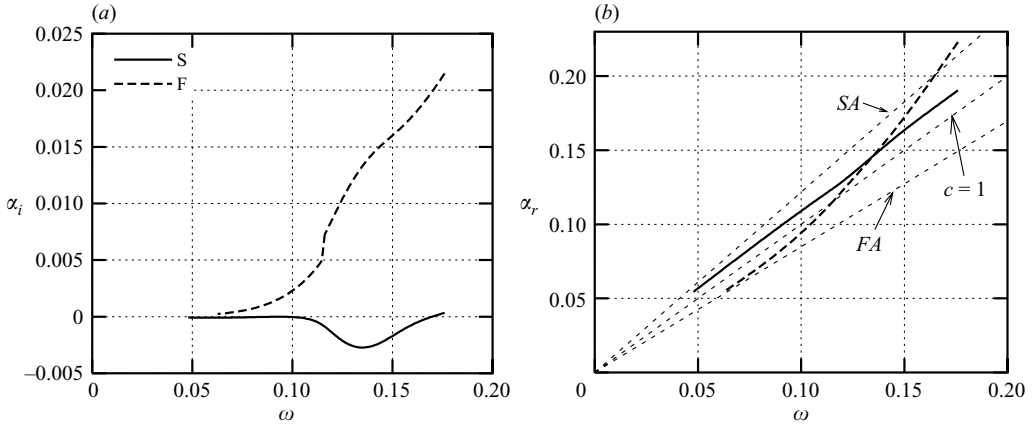


FIGURE 6. (a) Imaginary and (b) real parts of the wavenumber. $M = 5.6$, $Re = 704$, $F = 150 \times 10^{-6}$, $\beta = 5.77 \times 10^{-5}$.

imaginary, α_i , parts of the downstream wavenumber α versus the frequency. Lines SA and FA in figure 6(b) represent slow and fast acoustic modes with phase velocities $c = 1 \mp 1/M$, respectively. Figure 6(b) also shows the line corresponding to the phase velocity $c=1$ that represents vorticity and entropy perturbations moving with the free stream. One can see that at $\omega \rightarrow 0$ the discrete modes S and F are synchronized with the slow (SA) and the fast (FA) acoustic modes. This synchronization means that there is a channel of coupling between the acoustic and discrete modes.

At $\omega \approx 0.12$, the mode F is synchronized with the vorticity mode ($c=1$). This synchronization is accompanied by discontinuity in α_i . As was discussed by Fedorov & Tumin (2003), the discrete mode coalesces with the continuous spectrum from one side of the branch cut and reappears on the other side at another point. Mathematically, the pole associated with mode F approaches one side of the branch cut on the complex- p plane. At the same time, another pole, located on the lower Riemann sheet, approaches the branch cut. As the pole on the plane coalesces with the branch cut, it moves to the upper Riemann sheet while, simultaneously, the pole that was on the lower Riemann sheet moves into the complex- p plane at another point. The discontinuity of α_i at the point of synchronism between a discrete mode and the vorticity/entropy modes could also be seen in plots published by other authors (Mack 1969; Eißler & Bestek 1993). Usually, the discontinuity looks like a wiggle on the plots, and it has not been interpreted as a discontinuity. Balakumar & Malik (1992) reported coalescence of discrete modes with the vorticity/entropy branch cut in the complex plane α , but they did not report the reappearance of a discrete mode from another side.

There is a synchronism between mode F and mode S at $\omega \approx 0.13$. However, there is no coalescence of the eigenvalues. A model of two-mode synchronism considered in Fedorov & Khokhlov (1991) and Fedorov & Khokhlov (2001) explains branching of the modes at the point of synchronism. At this point, one of the modes becomes unstable, whereas the other one moves toward positive α_i . Although in this example the modes have the same value of $c_r \approx \omega/\alpha_r$ at $\omega \approx 0.13$, the minimum of $|\alpha_F - \alpha_S|$ exists in the vicinity of $\omega \approx 0.11$, and this is actually the point of the modes' branching. The synchronism between mode F and the vorticity/entropy modes accompanied by the synchronism between modes F and S suggests that there is a scenario associated with excitation of mode F by vorticity/entropy modes, and mode F can give rise to

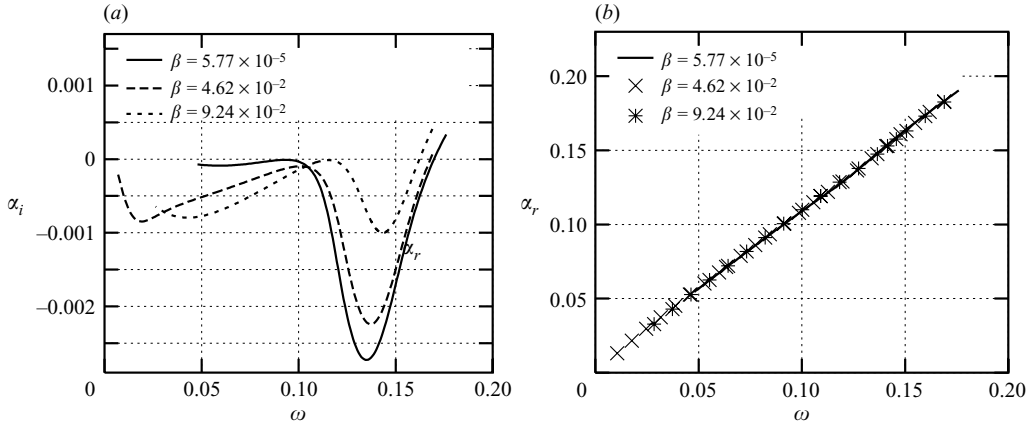


FIGURE 7. (a) Imaginary and (b) real parts of the wavenumber as functions of the frequency at $\beta = \text{const}$. Mode S. $M = 5.6$, $Re = 704$.

the unstable mode S at the point of their synchronism. The aforementioned properties of a discrete spectrum are typical for high Mach number ($M > 4$) and an adiabatic wall.

Figure 7(a, b) illustrates α_r and α_i for mode S as functions of frequency at three wavenumbers $\beta = 5.77 \times 10^{-5}$, 4.62×10^{-2} , and 9.24×10^{-2} . One can see from figure 7 that there is no significant effect on α_r , and that α_i has two minima. The first minimum (at lower ω) demonstrates that the mode is more unstable in the case of three-dimensional perturbations, whereas the magnitude of the second minimum decreases with an increase of β . Usually, these two peaks are associated with Mack's mode 1 and mode 2, respectively. This terminology originated from Mack's analysis of inviscid perturbations (Mack 1969). He found that an increase of Mach number is accompanied by an increase of distinct unstable discrete modes. Using asymptotic analysis, Gushchin & Fedorov (1989) showed that each amplified inviscid mode represents a separate solution. At finite Reynolds numbers, the structure of the discrete spectrum is different. Results in figure 7 correspond to one discrete normal mode, and the minima in α_i are only the footprints of Mack's mode 1 and mode 2.

4. Decomposition of three-dimensional perturbations

4.1. Examples when all components of the vector \mathbf{A}_0 are available

Recently, the multimode decomposition was successfully applied by Tumin *et al.* (2007) to an analysis of CFD data in the case of two-dimensional perturbations. The results of §2 and the orthogonality relation (B 6) provide a tool for decomposition of three-dimensional perturbations into normal modes of discrete and continuous spectra. To illustrate application of the method to three-dimensional perturbations, we emulate the 'CFD' data by superposition of modes from discrete and continuous spectra, and use the orthogonality condition in order to decompose the perturbation and to recover weights of the modes.

In the first example, we consider superposition of mode S, mode F, and a vorticity mode A in the boundary layer over a flat plate at $M = 5.95$, $T_w/T_{ad} = 0.1$. The frequency parameter $F = 10^{-4}$, the Reynolds number $Re = 1895$, and the spanwise wavenumber $\beta = 0.16$. The parameter k of the vorticity mode is equal to one. The eigenfunctions of these modes are normalized by the wall condition $\partial u / \partial y(0) = 1$.

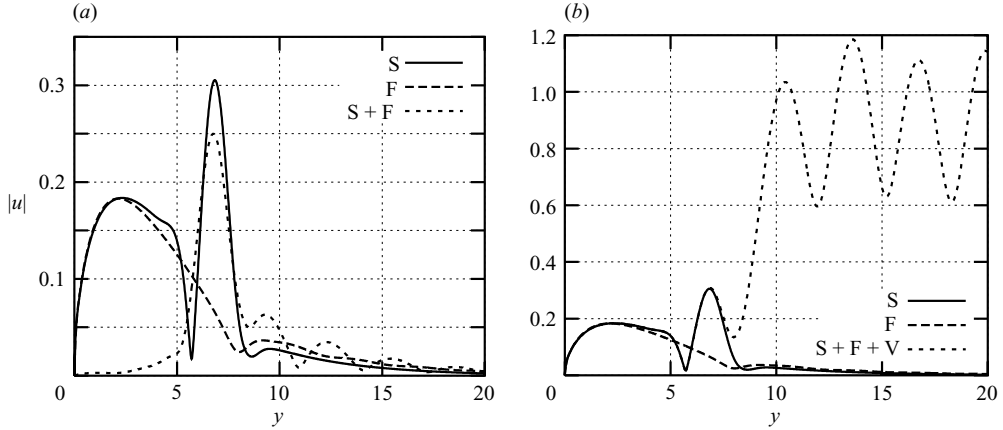


FIGURE 8. Superposition of mode S, mode F, and fast acoustic mode ($k=1$): (a) $C_S=1$, $C_F=-1$, $C_V=0$; (b) $C_S=1$, $C_F=-1$, $C_V=2$. $M=5.95$, $T_w/T_{ad}=0.1$, $F=10^{-4}$, $Re=1895$, $\beta=0.16$.

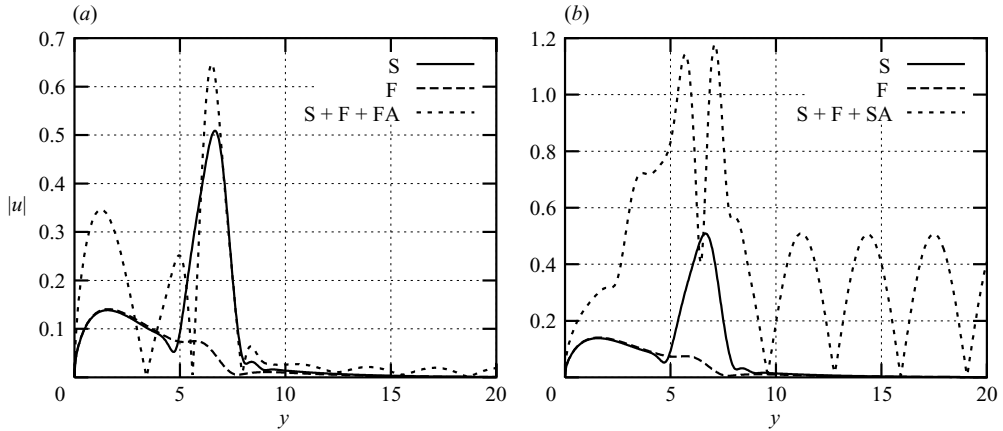


FIGURE 9. Superposition of mode S, mode F, and acoustic modes ($k=1$). (a) Two discrete modes and fast acoustic mode; (b) Two discrete modes and slow acoustic mode. $M=5.95$, $T_w/T_{ad}=0.1$, $F=10^{-4}$, $Re=2300$, $\beta=0.16$, $C_S=1$, $C_F=-1$, $C_{FA}=2$, $C_{SA}=2$.

Figure 8(a) shows superposition results of two discrete modes with weights $C_S=1$ and $C_F=-1$ for the slow and fast modes, respectively. Decomposition with the help of the orthogonality relation (B6) leads to the restored values of the coefficients $C_S=0.999996 + i5.55698 \times 10^{-7}$ and $C_F=-1.00001 + i1.78601 \times 10^{-6}$.

Figure 8(b) shows results when, in addition to the discrete modes as in figure 8(a), there is a vorticity mode with weight $C_V=2$. For this case, the decomposition with the help of the orthogonality relation (B6) leads to the coefficients $C_S=0.999999 + i1.21594 \times 10^{-6}$ and $C_F=-1.00002 - i3.90897 \times 10^{-6}$.

Examples of decomposition when the perturbations were composed of mode S ($C_S=1$), mode F ($C_F=-1$), and an acoustic wave are shown in figure 9(a,b). Figure 9(a) illustrates the case when the fast acoustic wave was used with $C_{FA}=2$, $k=1$, while the example with the slow acoustic wave ($C_{SA}=2$, $k=1$) is shown in figure 9(b). Results of the decomposition for the case corresponding to figure 9(a) were $C_S=0.999966 - i4.79233 \times 10^{-6}$ and $C_F=-1.00008 + i6.22089 \times 10^{-5}$. For the

example corresponding to figure 9(b), we found $C_S = 0.999948 - i 1.70326 \times 10^{-4}$ and $C_F = -0.999860 + i 1.87548 \times 10^{-4}$.

4.2. An example with partial data available

Similarly to the analysis of two-dimensional perturbations in Guydos & Tumin (2004), one can consider decomposition of three-dimensional perturbations when only partial information is available, as happens when experimental data are used. To proceed with the decomposition, one has to make an assumption about the modes input into the measured function. The accuracy of the assumption can be checked *a posteriori* by comparing the measured function to that constructed with the weights found from the decomposition.

Decomposition of steady three-dimensional perturbations into modes of continuous spectra is a more complicated problem because there are overlapping vorticity, entropy, and pressure (subsonic flow) modes of the continuous spectra. In the case of incompressible flow (Tumin 2003), the expansion into vorticity modes of the continuous spectra was approximated by a sum of the finite number of the modes with unknown coefficients that were found from a system of algebraic equations. The same algorithm, in principle, could be utilized for decomposition of perturbations into the vorticity modes of the continuous spectra in a compressible boundary layer. To illustrate the application, we consider a steady perturbation corresponding to optimal transiently growing disturbances at Mach number $M = 3$. We emulate the ‘measured’ velocity components and temperature perturbations by the solutions of the linearized boundary layer equations over a flat plate with an adiabatic wall (Tumin & Reshotko 2003). The Reynolds number is based on the free-stream velocity and the Blasius scale H is equal to 301.64. The spanwise wavenumber, β , is equal to 0.45.

For the purpose of this analysis, we assume that there is no influence from the upstream modes, and we carry out the decomposition only into two vorticity modes, A and B (see (2.32) and (2.33)) and entropy modes. For this type of perturbation (counter-rotating streamwise vortices), we assume that input from the acoustic branch cuts is negligible, and they are not included in the decomposition algorithm. For the present example, the continuous spectrum is discretized by 400 modes on the interval $k \in (0, 4)$.

Overlapping of the entropy and vorticity modes leads to significant complication of the algorithm. In order to avoid the overlapping, we used eigenfunctions of the continuous spectra at small ω . Figure 10(a) shows weight, $|C|$, for mode A obtained at $\omega = 10^{-4}$, 10^{-5} , and 5×10^{-6} to illustrate convergence as $\omega \rightarrow 0$. For the numerical decomposition into modes of the continuous spectra, in what follows, we use $\omega = 5 \times 10^{-6}$. The magnitudes of the weights for modes A and B and for entropy modes are shown in figure 10(b).

Figures 11(a, b) and 12 demonstrate a comparison of the x -, y -, z -velocity components, and temperature ‘measured’ and composed with the weights found for the vorticity and entropy modes. Similarly to the incompressible case (Tumin 2003), one can see that there is a discrepancy between the ‘measured’ and composed data of order $1/Re$.

5. Discussion of the results

The spatial Cauchy problem was solved for three-dimensional perturbations in compressible boundary layers. Although the numerical examples and the matrix elements in Appendix A were given for two-dimensional boundary layers, all the

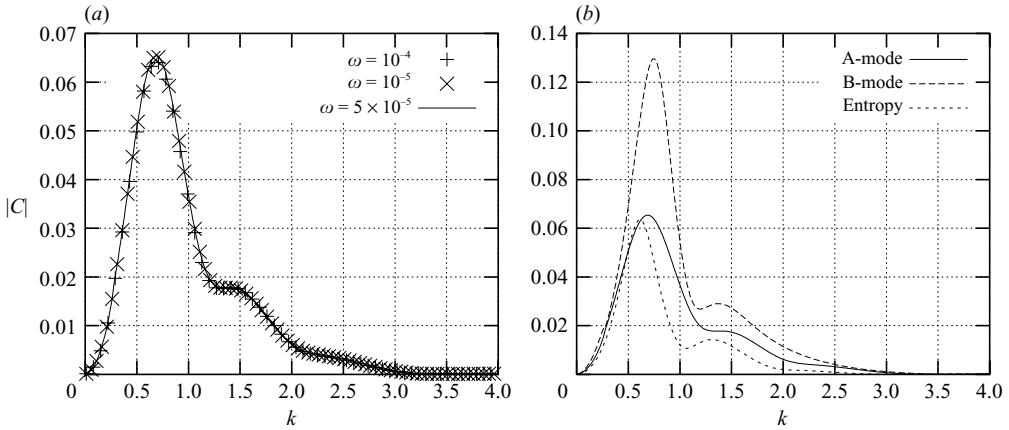


FIGURE 10. Vorticity and entropy modes in the multimode decomposition when three velocity components and temperature are ‘measured’: (a) Vorticity mode A at $\omega = 10^{-4}$, 10^{-5} , and 5×10^{-6} ; (b) Vorticity modes A and B and entropy mode at $\omega = 5 \times 10^{-6}$. $M = 3$, $Re = 301.64$, $\beta = 0.45$.

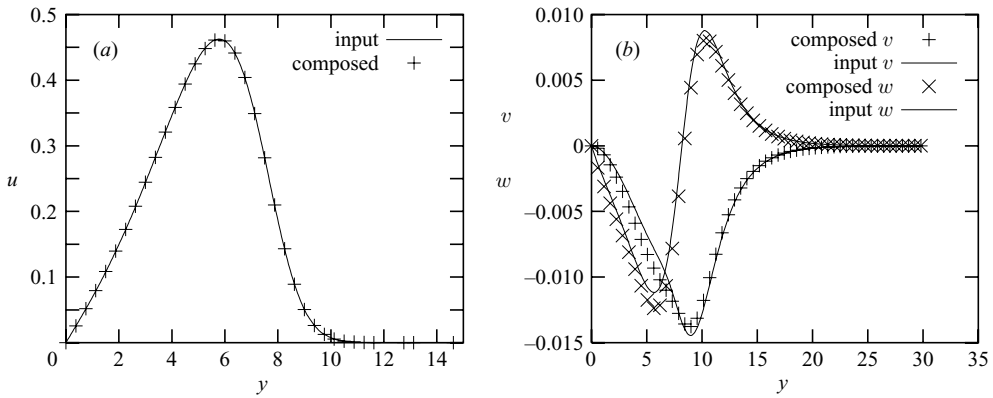


FIGURE 11. Comparison of ‘measured’ (input) and composed velocity components. $M = 3$, $Re = 301.64$, $\beta = 0.45$.

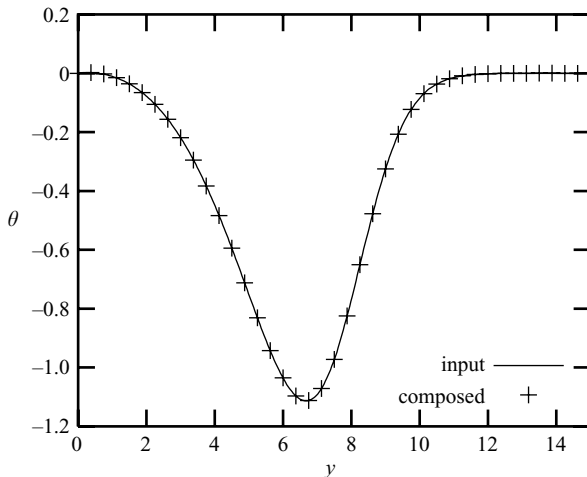


FIGURE 12. Comparison of ‘measured’ (input) and composed temperature perturbations. $M = 3$, $Re = 301.64$, $\beta = 0.45$.

results of §2 are valid (after minor adjustments in (2.25)) for three-dimensional boundary layers when the mean flow profiles are independent of the spanwise coordinate, z . These results provide a tool to decompose perturbations given only at a local station, x , into modes of continuous and discrete spectra. In order to be able to distinguish the modes, one needs amplitude and phase distributions for pressure, temperature, and velocity components, together with some of their derivatives with respect to the coordinate x . This is possible in computational studies of perturbations introduced into boundary layers, which might be helpful to elucidate underlying mechanisms that are important in laminar–turbulent transition scenarios. For example, we discussed in §3 the synchronism of discrete modes F and S. One of them might be unstable, and it could be responsible for transition to turbulence. The other decaying mode might be synchronized with vorticity and entropy modes. This means that there exists a route: ‘vorticity/entropy modes’ → ‘decaying discrete mode’ → ‘unstable discrete mode’ → ‘transition to turbulence’ (Fedorov & Khokhlov 2001). In conventional computational studies, the generation of the instability mode could only be observed in the far field, where the unstable mode dominates the other modes of discrete and continuous spectra. However, the significant element of the scenario – the decaying mode – could not be attained in the analysis. The present method allows evaluation of the amplitude of the decaying modes in order to provide a more rigorous background for interpretation of CFD results (Tumin *et al.* 2007).

Decomposition of perturbations when only partial information is available is an ill-posed problem. Nevertheless, one can apply a regularization procedure to recover the flow field. In fact, the assumption that the flow field is composed of downstream modes only is an example of regularization leading to decomposition based on measured velocity components and temperature only. We expect that developed methods of regularization for ill-posed problems (Tikhonov & Arsenin 1977; Tikhonov *et al.* 1995) may allow a further reduction of measured data under reasonable assumptions.

Although the examples considered are associated with the cases when the solution is composed of the downstream modes only, the orthogonality condition (B 6) allows distinguishing upstream modes in the initial data as well. The main constraint on the initial data is that they must be orthogonal to short-scale upstream modes in order to provide finite downstream growth rate for the solution, and to carry out the inverse Laplace transform.

The solution in the present work is based on the parallel flow approximation. This approximation is valid when the length scale of interest is much smaller than the characteristic scale of the unperturbed flow in the downstream direction. Results of the present work are also based on the assumption that the normalization constant Γ in (B 6) is not equal to zero. Fedorov & Khokhlov (2002) showed that the constant is equal to zero at the branching point of two discrete modes, and the non-parallel flow effects are to be taken into account in order to resolve the singularity. Analysis of discrete and continuous spectra by Tumin *et al.* (2007) demonstrated that the normalization constant tends to zero also in the case of synchronism between the discrete mode and the continuous spectra. Therefore, an extension of the theoretical model by Fedorov & Khokhlov (2002) is required when one needs to resolve the mode close to a point of synchronism with the continuous spectra.

Another issue that we find worthwhile to address in this discussion is the terminology used for discrete modes in high-speed boundary layers. Historically, the terminology was introduced by Mack (1969). In his inviscid analysis of perturbations, Mack discovered the existence of new instability modes. At finite Reynolds numbers (see our example in §3), there is only one unstable mode having signatures of Mack’s

mode 1 and mode 2 (see figure 7a). Mathematically, this is a single mode associated with a pole in the solution (2.27), and the pole is moving around the complex plane in such a way that one can see two peaks in the imaginary part of α . (Balakumar & Malik (1992) also emphasized that there exists only one unstable eigenvalue, α , for a given β .) These two peaks are associated with Mack's mode 1 and 2. The first peak demonstrates that three-dimensional perturbations grow faster than two-dimensional, whereas the second peak has the opposite trend. One should keep in mind that the terminology based on Mack's modes addresses different behaviours of the same unstable mode at low and high frequencies.

This work was sponsored by the Air Force Office of Scientific Research, USAF under grant No. FA9550-05-101 monitored by Dr J. D. Schmisser. The views and conclusions contained herein are those of the author and should not be interpreted as necessarily representing the official policies or endorsements, either expressed or implied, of the Air Force Office of Scientific Research or the US Government.

Appendix A. The matrix elements

In what follows, U_s , T_s , and μ_s are velocity, temperature, and viscosity of the mean flow, respectively, and they are scaled with their values at the edge of the boundary layer. The pressure is scaled with $\rho_e U_e^2$, and $\mu'_s = d\mu/dT_s$; Re , Pr , and γ are the Reynolds number, Prandtl number, and specific heat ratio, respectively; M is the Mach number at the edge of the boundary layer; $D = d/dy$. The parameters r and m are defined as $r = 2(e + 2)/3$ and $m = 2(e - 1)/3$, and $2e/3$ is the ratio of the bulk viscosity to the dynamic viscosity. In particular, Stokes' hypothesis corresponds to $e = 0$.

Non-zero elements of the matrices in (2.1) are

$$\begin{aligned}
 L_0^{43} &= -\frac{r\mu_s}{Re}, \\
 L_1^{11} &= L_1^{22} = L_1^{33} = L_1^{44} = L_1^{55} = L_1^{66} = L_1^{77} = L_1^{88} = 1, \\
 L_1^{2,10} &= L_1^{8,14} = m + 1. \\
 H_1^{12} &= 1, \quad H_1^{21} = -\frac{i\omega Re}{T_s\mu_s}, \quad H_1^{22} = -\frac{D\mu_s}{\mu_s}, \quad H_1^{23} = \frac{ReDU}{T_s\mu_s}, \\
 H_1^{25} &= -\frac{D(\mu'_s DU)}{\mu_s}, \quad H_1^{26} = -\frac{\mu'_s DU}{\mu_s}, \\
 H_1^{33} &= \frac{DT_s}{T_s}, \quad H_1^{34} = i\omega\gamma M^2, \quad H_1^{35} = -\frac{i\omega}{T_s}, \\
 H_1^{43} &= i\omega\rho_s, \quad H_1^{56} = 1, \\
 H_1^{62} &= -2(\gamma - 1)Pr M^2 DU_s, \quad H_1^{63} = \frac{RePr}{T_s\mu_s} DT_s, \\
 H_1^{64} &= i\omega(\gamma - 1)\frac{RePr}{\mu_s} M^2, \\
 H_1^{65} &= -i\omega\frac{RePr}{T_s\mu_s} - (\gamma - 1)\frac{Pr}{\mu_s} M^2 \mu'_s \left(\frac{\partial U_s}{\partial y}\right)^2 - \frac{D(\mu'_s DT_s)}{\mu_s}, \\
 H_1^{66} &= -\frac{2D\mu_s}{\mu_s},
 \end{aligned}$$

$$\begin{aligned}
H_1^{78} &= 1, \quad H_1^{87} = -\frac{i\omega Re}{\mu_s T_s}, \quad H_1^{88} = -\frac{D\mu_s}{\mu_s}, \\
H_1^{99} &= H_1^{10,10} = H_1^{11,11} = H_1^{12,12} = H_1^{13,13} = H_1^{14,14} = H_1^{15,15} = H_1^{16,16} = -1. \\
H_2^{21} &= \frac{Re}{T_s \mu_s} U_s, \quad H_2^{23} = -\frac{D\mu_s}{\mu_s}, \quad H_2^{24} = \frac{Re}{\mu_s}, \quad H_2^{29} = -r, \\
H_2^{31} &= -1, \quad H_2^{34} = -\gamma U_s M^2, \quad H_2^{35} = \frac{U_s}{T_s}, \\
H_2^{41} &= \frac{mD\mu_s}{Re}, \quad H_2^{42} = (m+1)\frac{\mu_s}{Re}, \quad H_2^{43} = -\frac{U_s}{T_s}, \quad H_2^{45} = \frac{\mu'_s}{Re} DU_s, \quad H_2^{4,10} = \frac{\mu_s}{Re}, \\
H_2^{63} &= -2(\gamma-1)Pr M^2 DU_s, \quad H_2^{64} = -(\gamma-1)\frac{RePr}{\mu_s} M^2 U_s, \\
H_2^{65} &= \frac{RePr}{T_s \mu_s} U_s, \quad H_2^{6,11} = -1, \\
H_2^{87} &= \frac{ReU_s}{\mu_s T_s}, \quad H_2^{8,12} = -1, \quad H_2^{8,13} = -(m+1), \\
H_2^{9,1} &= H_2^{10,3} = H_2^{11,5} = H_2^{12,7} = 1. \\
H_3^{2,12} &= -(m+1), \quad H_3^{2,13} = -1, \quad H_3^{37} = -1, \\
H_3^{47} &= \frac{mD\mu_s}{Re}, \quad H_3^{48} = (m+1)\frac{\mu_s}{Re}, \quad H_3^{4,14} = \frac{\mu_s}{Re}, \quad H_3^{6,15} = -1, \\
H_3^{83} &= -\frac{D\mu_s}{\mu_s}, \quad H_3^{84} = \frac{Re}{\mu_s}, \quad H_3^{8,16} = -r, \\
H_3^{13,1} &= H_3^{14,3} = H_3^{15,5} = H_3^{16,7} = 1.
\end{aligned}$$

One can also find the non-zero elements of the matrix \mathbf{H}_0 in (B3) and (B4) from Nayfeh (1980) with the spanwise velocity of the mean flow equal to zero, $\alpha = -ip$, and

$$\begin{aligned}
\hat{\omega} &= \omega - \alpha U_s, & \chi &= \left[\frac{Re}{\mu_s} - ir\gamma M^2 \hat{\omega} \right]^{-1}. \\
H_0^{12} &= H_0^{56} = H_0^{78} = 1, \\
H_0^{21} &= \alpha^2 + \beta^2 - i\hat{\omega} \frac{Re}{\mu_s T_s}, \quad H_0^{22} = -\frac{D\mu_s}{\mu_s}, \\
H_0^{23} &= -i\alpha(m+1)\frac{DT_s}{T_s} - i\alpha \frac{D\mu_s}{\mu_s} + Re \frac{DU_s}{\mu_s T_s}, \\
H_0^{24} &= i\alpha \frac{Re}{\mu_s} + (m+1)\gamma M^2 \alpha \hat{\omega}, \quad H_0^{25} = -\alpha(m+1)\frac{\hat{\omega}}{T_s} - \frac{D(\mu'_s DU_s)}{\mu_s}, \\
H_0^{26} &= -\frac{\mu'_s DU_s}{\mu_s}, \\
H_0^{31} &= -i\alpha, \quad H_0^{33} = \frac{DT_s}{T_s}, \quad H_0^{34} = i\gamma M^2 \hat{\omega}, \quad H_0^{35} = -\frac{i\hat{\omega}}{T_s}, \quad H_0^{37} = -i\beta, \\
H_0^{41} &= -i\chi\alpha \left(r \frac{DT_s}{T_s} + 2 \frac{D\mu_s}{\mu_s} \right), \quad H_0^{42} = -i\chi\chi, \\
H_0^{43} &= \chi \left[-\alpha^2 - \beta^2 + i \frac{\hat{\omega} Re}{\mu_s T_s} + r \frac{D^2 T_s}{T_s} + r \frac{D\mu_s DT_s}{\mu_s T_s} \right],
\end{aligned}$$

$$\begin{aligned}
 H_0^{44} &= -i\chi r\gamma M^2 \left[\alpha DU_s - \hat{\omega} \frac{DT_s}{T_s} - \hat{\omega} \frac{D\mu_s}{\mu_s} \right], \\
 H_0^{45} &= i\chi \left[r \frac{\alpha DU_s}{T_s} + \frac{\mu'_s}{\mu_s} \alpha DU_s - r \hat{\omega} \frac{D\mu_s}{\mu_s T_s} \right], \\
 H_0^{46} &= -i\chi r \frac{\hat{\omega}}{T_s}, \quad H_0^{47} = -i\chi\beta \left(r \frac{DT_s}{T_s} + 2 \frac{D\mu_s}{\mu_s} \right), \quad H_0^{48} = -i\beta\chi, \\
 H_0^{62} &= -2(\gamma - 1)M^2 Pr DU_s, \\
 H_0^{63} &= -2i(\gamma - 1)M^2 Pr \alpha DU_s + Re Pr \frac{DT_s}{\mu_s T_s}, \\
 H_0^{64} &= i(\gamma - 1)M^2 Pr Re \frac{\hat{\omega}}{\mu_s}, \\
 H_0^{65} &= \alpha^2 + \beta^2 - iRe Pr \frac{\hat{\omega}}{\mu_s T_s} - (\gamma - 1)M^2 Pr \mu'_s \frac{(DU_s)^2}{\mu_s} - \frac{D^2 \mu_s}{\mu_s}, \\
 H_0^{66} &= -2 \frac{D\mu_s}{\mu_s}, \quad H_0^{83} = -i(m + 1)\beta \frac{DT_s}{T_s} - i\beta \frac{D\mu_s}{\mu_s}, \\
 H_0^{84} &= (m + 1)\gamma M^2 \beta \hat{\omega} + \frac{i\beta Re}{\mu_s}, \\
 H_0^{85} &= -(m + 1) \frac{\beta \hat{\omega}}{T_s}, \\
 H_0^{87} &= \alpha^2 + \beta^2 - \frac{i\hat{\omega} Re}{\mu_s T_s}, \quad H_0^{88} = -\frac{D\mu_s}{\mu_s}.
 \end{aligned}$$

Appendix B. The biorthogonal eigenfunction system

We introduce the following biorthogonal eigenfunction system $\{\mathbf{A}_{\alpha\beta}, \mathbf{B}_{\alpha\beta}\}$:

$$\frac{\partial}{\partial y} \left(\mathbf{L}_0 \frac{\partial \mathbf{A}_{\alpha\beta}}{\partial y} \right) + \mathbf{L}_1 \frac{\partial \mathbf{A}_{\alpha\beta}}{\partial y} = \mathbf{H}_1 \mathbf{A}_{\alpha\beta} + i\alpha \mathbf{H}_2 \mathbf{A}_{\alpha\beta} + i\beta \mathbf{H}_3 \mathbf{A}_{\alpha\beta}, \quad (\text{B } 1)$$

$$y = 0: \quad A_{\alpha\beta 1} = A_{\alpha\beta 3} = A_{\alpha\beta 5} = A_{\alpha\beta 7} = 0,$$

$$y \rightarrow \infty: \quad |A_{\alpha\beta j}| < \infty,$$

$$\frac{\partial}{\partial y} \left(\mathbf{L}_0^T \frac{\partial \mathbf{B}_{\alpha\beta}}{\partial y} \right) - \mathbf{L}_1^T \frac{\partial \mathbf{B}_{\alpha\beta}}{\partial y} = \mathbf{H}_1^T \mathbf{B}_{\alpha\beta} + i\alpha \mathbf{H}_2^T \mathbf{B}_{\alpha\beta} + i\beta \mathbf{H}_3^T \mathbf{B}_{\alpha\beta}, \quad (\text{B } 2)$$

$$y = 0: \quad B_{\alpha\beta 2} = B_{\alpha\beta 4} = B_{\alpha\beta 6} = B_{\alpha\beta 8} = 0,$$

$$y \rightarrow \infty: \quad |B_{\alpha\beta j}| < \infty.$$

Equation (B 2) defines the complex conjugate of the conventional adjoint problem.

Equation (B 1) can be recast as a system of eight ODEs,

$$\frac{d\mathbf{z}_{\alpha\beta}}{dy} = \mathbf{H}_0 \mathbf{z}_{\alpha\beta}, \quad (\text{B } 3)$$

where vector $\mathbf{z}_{\alpha\beta}$ is comprised of the first eight elements of the vector $\mathbf{A}_{\alpha\beta}$. The conventional adjoint problem in three-dimensional stability equations is found from the following system of ODEs:

$$-\frac{d\mathbf{Y}_{\alpha\beta}}{dy} = \mathbf{H}_0 \mathbf{Y}_{\alpha\beta}. \quad (\text{B } 4)$$

One can establish correspondence between $\mathbf{B}_{\alpha\beta}$ and $\mathbf{Y}_{\alpha\beta}$ similar to the case of temporal three-dimensional normal modes (FT):

$$B_{\alpha\beta 1} = Y_{\alpha\beta 1} + \frac{i\alpha L_0^{43} Y_{\alpha\beta 4}}{(1 + L_0^{43} H_0^{34})}, \quad B_{\alpha\beta 2} = Y_{\alpha\beta 2}, \quad (\text{B } 5a, b)$$

$$B_{\alpha\beta 3} = Y_{\alpha\beta 3} - i\alpha(m+1)Y_{\alpha\beta 2} - i\beta(m+1)Y_{\alpha\beta 8} - \frac{L_0^{43} H_0^{33} Y_{\alpha\beta 4}}{(1 + L_0^{43} H_0^{34})} + L_0^{43} \frac{d}{dy} \left[\frac{Y_{\alpha\beta 4}}{(1 + L_0^{43} H_0^{34})} \right], \quad (\text{B } 5c)$$

$$B_{\alpha\beta 4} = \frac{Y_{\alpha\beta 4}}{(1 + L_0^{43} H_0^{34})}, \quad B_{\alpha\beta 5} = Y_{\alpha\beta 5} + H_0^{46} Y_4, \quad B_{\alpha\beta 6} = Y_{\alpha\beta 6}, \quad (\text{B } 5d-f)$$

$$B_{\alpha\beta 7} = Y_{\alpha\beta 7} + \frac{i\beta L_0^{43} Y_{\alpha\beta 4}}{(1 + L_0^{43} H_0^{34})}, \quad B_{\alpha\beta 8} = Y_{\alpha\beta 8}, \quad B_{\alpha\beta 9} = -i\alpha r B_{\alpha\beta 2}, \quad (\text{B } 5g-i)$$

$$B_{\alpha\beta 10} = (m+1) \frac{dB_{\alpha\beta 2}}{dy} + i\alpha H_2^{4,10} B_{\alpha\beta 4}, \quad B_{\alpha\beta 11} = -i\alpha B_{\alpha\beta 6}, \quad (\text{B } 5j, k)$$

$$B_{\alpha\beta 12} = -i\alpha B_{\alpha\beta 8} - i\beta(m+1)B_{\alpha\beta 2}, \quad B_{\alpha\beta 13} = -i\alpha(m+1)B_{\alpha\beta 8} - i\beta B_{\alpha\beta 2}, \quad (\text{B } 5l, m)$$

$$B_{\alpha\beta 14} = (m+1) \frac{dB_{\alpha\beta 8}}{dy} + i\beta H_3^{4,14} B_{\alpha\beta 4}, \quad B_{\alpha\beta 15} = -i\beta B_{\alpha\beta 6}, \quad B_{\alpha\beta 16} = -i\beta r B_{\alpha\beta 8}, \quad (\text{B } 5n-p)$$

where r and m are defined in Appendix A.

The eigenfunction system $\{\mathbf{A}_{\alpha\beta}, \mathbf{B}_{\alpha\beta}\}$ has an orthogonality relation given as

$$\langle \mathbf{H}_2 \mathbf{A}_{\alpha\beta}, \mathbf{B}_{\alpha'\beta} \rangle \equiv \int_0^\infty (\mathbf{H}_2 \mathbf{A}_{\alpha\beta}, \mathbf{B}_{\alpha'\beta}) dy = \Gamma \Delta_{\alpha\alpha'}, \quad (\text{B } 6)$$

where Γ is a normalization constant; $\Delta_{\alpha\alpha'}$ is a Kronecker delta if either α or α' belongs to the discrete spectrum; $\Delta_{\alpha\alpha'}$ is a Dirac delta function if both α and α' belong to the continuous spectrum. Because (B 2) represents the complex conjugate of the conventional problem, the dot product $(,)$ in (B 6) does not involve complex conjugation. One can also establish the following equality:

$$\langle \mathbf{H}_2 \mathbf{A}_{\alpha\beta}, \mathbf{B}_{\alpha\beta} \rangle = -i \left\langle \frac{\partial \mathbf{H}_0}{\partial \alpha} \mathbf{z}_{\alpha\beta}, \mathbf{Y}_{\alpha\beta} \right\rangle. \quad (\text{B } 7)$$

In our computations of the adjoint eigenfunctions, we find $\mathbf{Y}_{\alpha\beta}$ from (B 4) and restore $\mathbf{B}_{\alpha\beta}$ with the help of (B 5). Because the derivation of asymptotic fundamental solutions of (B 4) as $y \rightarrow \infty$ is too complicated, we utilize the theorem (Kamke 1959) that fundamental solutions of the adjoint system (B 4) can be found as vectors ξ_j composed of cofactors of the j th column in the matrix of fundamental solution, \mathbf{m} , defined in (2.15). Therefore, we do not derive the asymptotics, but find them numerically with the help of the known asymptotic result for the matrix \mathbf{m} . Utilizing asymptotics for \mathbf{z}_j (see Appendix C), one can find asymptotics ξ_j as follows:

$$\left. \begin{aligned} \xi_1 &= \xi_1^0 e^{\lambda_2 y}, & \xi_2 &= \xi_2^0 e^{\lambda_1 y}, & \xi_3 &= \xi_3^0 e^{\lambda_4 y}, & \xi_4 &= \xi_4^0 e^{\lambda_3 y}, \\ \xi_5 &= \xi_5^0 e^{\lambda_6 y}, & \xi_6 &= \xi_6^0 e^{\lambda_5 y}, & \xi_7 &= \xi_7^0 e^{\lambda_8 y}, & \xi_8 &= \xi_8^0 e^{\lambda_7 y}. \end{aligned} \right\} \quad (\text{B } 8)$$

For each fundamental solution ξ_j having 8 components, one can restore fundamental solutions ζ_j for the adjoint problem (B 2) composed of 16 components with the help of (B 5). These steps allow computation of the adjoint eigenfunctions $\mathbf{B}_{\alpha\beta}$ of the discrete and continuous spectra.

One can find the following presentation of the adjoint eigenvectors \mathbf{B}_c corresponding to the continuous spectra:

$$\mathbf{B}_{c,1} = \zeta_1 E_{1753} + \zeta_2 E_{2753} + \zeta_4 E_{4753} + \zeta_6 E_{6753} + \zeta_8 E_{8753}, \quad (\text{B } 9)$$

$$\mathbf{B}_{c,2} = \zeta_1 E_{1283} - \zeta_4 E_{2834} + \zeta_5 E_{2853} + \zeta_6 E_{2863} - \zeta_7 E_{2783}, \quad (\text{B } 10)$$

$$\mathbf{B}_{c,3} = \zeta_1 E_{6218} - \zeta_3 E_{2863} + \zeta_4 E_{2468} - \zeta_5 E_{6528} - \zeta_7 E_{6728}, \quad (\text{B } 11)$$

$$\mathbf{B}_{c,4} = \zeta_2 E_{1275} + \zeta_3 E_{1753} + \zeta_4 E_{1754} + \zeta_6 E_{1756} + \zeta_8 E_{7185}, \quad (\text{B } 12)$$

$$\mathbf{B}_{c,5} = \zeta_1 E_{1253} + \zeta_4 E_{5234} + \zeta_6 E_{2563} + \zeta_7 E_{7253} + \zeta_8 E_{8253}. \quad (\text{B } 13)$$

For the discrete modes, we find

$$\mathbf{B}_v = \zeta_2 E_{1257} + \zeta_4 E_{1457} + \zeta_6 E_{1765} + \zeta_8 E_{1578}. \quad (\text{B } 14)$$

One can see that the coefficients in (2.30), (2.32), (2.33), (2.35), (2.37), and (2.39), depending on the initial conditions, are associated with the adjoint eigenvectors, respectively, as follows:

$$\left. \begin{aligned} c_2 E_{1275} + c_3 E_{1753} + c_4 E_{1754} + c_6 E_{1756} + c_8 E_{7185} &\sim \langle \mathbf{H}_2 \mathbf{A}_0, \mathbf{B}_{c,4} \rangle, \\ c_1 E_{1753} + c_2 E_{2753} + c_4 E_{4753} + c_6 E_{6753} + c_8 E_{8753} &\sim \langle \mathbf{H}_2 \mathbf{A}_0, \mathbf{B}_{c,1} \rangle, \\ c_1 E_{1253} + c_4 E_{5234} + c_6 E_{2563} + c_7 E_{7253} + c_8 E_{8253} &\sim \langle \mathbf{H}_2 \mathbf{A}_0, \mathbf{B}_{c,5} \rangle, \\ c_1 E_{1283} - c_4 E_{2834} + c_5 E_{2853} + c_6 E_{2863} - c_7 E_{2783} &\sim \langle \mathbf{H}_2 \mathbf{A}_0, \mathbf{B}_{c,2} \rangle, \\ c_1 E_{6218} - c_3 E_{2863} + c_4 E_{2468} - c_5 E_{6528} - c_7 E_{6728} &\sim \langle \mathbf{H}_2 \mathbf{A}_0, \mathbf{B}_{c,3} \rangle, \\ c_2 E_{1257} + c_4 E_{1457} + c_6 E_{1765} + c_8 E_{1578} &\sim \langle \mathbf{H}_2 \mathbf{A}_0, \mathbf{B}_v \rangle. \end{aligned} \right\} \quad (\text{B } 15)$$

Following Salwen & Grosch (1981), one can prove that the inverse Laplace transform (2.40) is an expansion into the biorthogonal eigenfunction system $\{\mathbf{A}_{\alpha\beta}, \mathbf{B}_{\alpha\beta}\}$.

The asymptotic vectors \mathbf{Z}_j^0 and ζ_j^0 are used to calculate the normalization constant, Γ , in the orthogonality relation (B 6) for the continuous spectra. Evaluation of the normalization constant Γ for the continuous spectra can be found with the help of integrals like $\int_0^\infty \exp(i(k - k')y) dy = \pi \delta(k - k')$ (Tumin 2003). For example, one can find for an acoustic mode

$$\Gamma = \pi [(\mathbf{H}_2 \mathbf{Z}_5^0, \zeta_5^0) + (\mathbf{H}_2 \mathbf{Z}_6^0, \zeta_6^0)]. \quad (\text{B } 16)$$

Appendix C. Numerical method

Two independent codes were used in the present work. The first one (SCM) was based on the single-domain Chebyshev spectral collocation method (Malik 1990). Solution of the linearized Navier–Stokes equations for compressible gas is considered in the wave-like form

$$(u, v, w, \pi, \theta) = (\hat{u}(y), \hat{v}(y), \hat{w}(y), \hat{\pi}(y), \hat{\theta}(y)) e^{i(\alpha x + \beta z - \omega t)}. \quad (\text{C } 1)$$

In order to avoid the nonlinearity in α , we introduce the vector

$$\Phi = (\hat{u}, \hat{v}, \hat{w}, \hat{\pi}, \hat{\theta}, i\alpha \hat{u}, i\alpha \hat{v}, i\alpha \hat{w}, i\alpha \hat{\theta})^T, \quad (\text{C } 2)$$

and the system of ODEs for the amplitude functions is written in the matrix form

$$(A_1 D^2 + A_2 D + A_3) \Phi = \alpha A_4 \Phi, \quad (\text{C } 3)$$

where $D = d/dy$; A_1, A_2, A_3 , and A_4 are 9×9 matrices.

Homogeneous boundary conditions for (C 3) are formulated on the wall, $y = 0$, and at $y = y_{max}$,

$$y = 0 \quad \text{and} \quad y \rightarrow \infty: \quad \Phi_j = 0 \quad (j = 1, 2, 3, 5, \dots, 9). \quad (\text{C } 4)$$

In the numerical implementation, the boundary conditions (C 4) were supplemented by the y -momentum equation at $y = 0$ and $y = y_{max}$.

An algebraic stretching was employed in order to map interval $[0, y_{max}]$ onto the Chebyshev interval $\xi \in [-1, +1]$,

$$y = d \frac{1 + \xi}{b - \xi}, \quad (\text{C } 5)$$

where $b = 1 + 2d/y_{max}$ and $d = y_i y_{max}/(y_{max} - 2y_i)$. The parameter y_i is chosen to locate half of the grid points in the interval $(0, y_i)$. The N th-order Chebyshev polynomials T_N were used with the collocation points

$$\xi_j = \cos(\pi j/N), \quad j = 0, \dots, N. \quad (\text{C } 6)$$

The unknown functions and their derivatives at the collocation points, y_j , are presented as sums of the Chebyshev polynomials, T_n , with unknown coefficients, a_n :

$$Q(y_j) = \sum_{n=0}^N a_n T_n(y_j), \quad (\text{C } 7)$$

As a result of the discretization, we arrive at the generalized eigenvalue problem

$$A_g \tilde{a} = \alpha B_g \tilde{a}, \quad (\text{C } 8)$$

where A_g and B_g are $9(N + 1) \times 9(N + 1)$ matrices, and \tilde{a} is the vector composed of $9(N + 1)$ unknown coefficients. Because the rows of the matrix B_g corresponding to the boundary conditions (C 4) contain only zeros, we replace them by the corresponding rows of the matrix A_g divided by a large number, as was suggested by Hanifi, Schmid & Henningson (1996). This introduces eigenvalues that are located far away from the domain of interest in the complex plane α . The generalized eigenvalue problem (C 8) was solved with the help of standard routine DG6CCG from the IMSL FORTRAN Library.

Malik (1990) reported eigenvalue $\alpha = 0.2534048 - i0.0024921$ for a two-dimensional perturbation in a boundary layer over a flat plate with an adiabatic wall. The following parameters were used: Mach number $M = 4.5$; the Reynolds number $Re = 1500$ was based on the Blasius scale; the stagnation temperature $T_0 = 611.11$ K; and the Prandtl number $Pr = 0.70$. For these parameters, we considered three-dimensional perturbations at $\beta = 10^{-4}$. At $N = 125$, $y_i = 5$, and $y_{max} = 100$, our result was $\alpha = 0.2534416 - i0.0027743$. Variation of y_i and y_{max} did not reveal a difference within six digits. Increasing N up to 175 revealed an effect only on the last digits of the real and imaginary parts of α . This code had an auxiliary role, and it served for verification of the other code that was based on the fourth-order Runge–Kutta solver for equations (B 3) and (B 4), and to provide an initial guess for the eigenvalues.

In the second code (RK), the fundamental solutions of equations (B 3) and (B 4) were found numerically by integration of the equations from y_{max} to the wall with the known analytical asymptotic solutions outside the boundary layer, $z_j^0 \exp(\lambda_j y)$. One can find the asymptotic vectors z_j^0 from (B 3) as $y \rightarrow \infty$. For vectors $z_{1,2}^0$ and $z_{7,8}^0$,

Balakumar & Malik (1992), $\beta = 0$	The present work, $\beta = 10^{-4}$
(0.220, -3.091×10^{-3})	(0.220, -3.091×10^{-3})
(0.221, 1.569×10^{-2})	(0.221, 1.569×10^{-2})
(-0.565 , 5.559×10^{-2})	(-0.565 , 5.560×10^{-2})
(0.560, 5.659×10^{-1})	(0.561, 5.659×10^{-1})

TABLE 1. Flat plate. $M = 4.5$, $T_0 = 311$ K, $Pr = 0.72$, $Re = 1000$, $\omega = 0.2$

we have

$$\mathbf{z}_{1,2}^0 = (1, \lambda_{1,2}, H_0^{31}/\lambda_{1,2}, 0, 0, 0, 0, 0)^T, \tag{C 9}$$

$$\mathbf{z}_{7,8}^0 = (0, 0, H_0^{37}/\lambda_{7,8}, 0, 0, 0, 1, \lambda_{7,8})^T, \tag{C 10}$$

where the matrix elements H_0^{ij} are defined in Appendix A.

The non-zero elements z_{ij}^0 of vectors \mathbf{z}_j^0 ($j = 3, \dots, 6$) were calculated as follows:

$$z_{1j}^0 = 1, \quad z_{2j}^0 = \lambda_j, \quad z_{4j}^0 = (\lambda_j^2 - H_0^{21})b_{23}/b_{12}, \tag{C 11a}$$

$$z_{5j}^0 = -(b_{22} - \lambda_j^2)(\lambda_j^2 - H_0^{21})/b_{12}, \quad z_{6j}^0 = \lambda_j z_{6j}^0, \tag{C 11b}$$

$$z_{7j}^0 = (H_0^{84}z_{4j}^0 + H_0^{85}z_{5j}^0)/(\lambda_j^2 - H_0^{87}), \quad z_{8j}^0 = \lambda_j z_{7j}^0, \tag{C 11c}$$

$$z_{3j}^0 = (H_0^{31}z_{1j}^0 + H_0^{34}z_{4j}^0 + H_0^{35}z_{5j}^0 + H_0^{37}z_{7j}^0)/\lambda_j, \tag{C 11d}$$

where $b_{12} = H_0^{24}b_{23} - H_0^{25}(b_{22} - \lambda_j^2)$, and b_{22} and b_{23} are defined in (2.11).

Asymptotic vectors ξ_j^0 for the system (B 4) were found numerically from the matrix of the fundamental solutions \mathbf{m} introduced in (2.15) (see discussion of properties of the adjoint system in Appendix B). The Gram–Schmidt orthonormalization procedure was employed in the computation of the fundamental solutions \mathbf{z}_j and ξ_j during integration across the boundary layer.

Finally, the eigenfunctions of the direct and adjoint problems could be obtained as a sum of the fundamental solutions with unknown coefficients that are to be determined from the boundary conditions on the wall. In the case of continuous spectra, the eigenfunctions are composed of five fundamental solutions. The unknown coefficients could be found from four boundary conditions on the wall ($\hat{u} = \hat{v} = \hat{w} = \hat{\theta} = 0$) and the normalization condition $d\hat{u}/dy(0) = 1$. The wavenumbers α corresponding to the modes of the continuous spectra were found from the equation $\lambda_j^2 = -k^2$. For the problem of the discrete spectrum, the eigenfunctions are composed of four fundamental solutions $\mathbf{z}_1, \mathbf{z}_3, \mathbf{z}_5$, and \mathbf{z}_7 . The four unknown coefficients were determined from the boundary conditions $\hat{u} = \hat{v} = \hat{w} = 0$ and the normalization condition $d\hat{u}/dy(0) = 1$. The eigenvalue α was found with the help of the Newton method as a root of the equation $\theta(0) = 0$. The convergence criterion was chosen as $|\theta(0)| < \varepsilon$ with $\varepsilon \leq 10^{-5}$.

We tested the code with the example discussed above. The outer boundary was chosen as $y_{max} = 35$, with the uniform grid having $N = 601$ nodes and the convergence criterion $\varepsilon = 10^{-5}$. The spanwise wavenumber β was held at 10^{-4} . The eigenvalue found was $\alpha = 0.2534420 - i0.0027738$. The result remained the same for $N = 1201$, $\varepsilon = 10^{-5}$, and $N = 601$, $\varepsilon = 10^{-7}$.

In another test, we used the eigenvalues reported by Balakumar & Malik (1992) for a boundary layer over an adiabatic flat plate at Mach number $M = 4.5$, Prandtl number $Pr = 0.72$, stagnation temperature in the free stream $T_0 = 311$ K, Reynolds number $Re = 1000$, and dimensionless frequency $\omega = 0.2$. In table 1, we compare our

Balakumar & Malik (1992)	The present work
(0.2181, 2.969×10^{-4})	(0.2181, 2.974×10^{-4})
(0.2124, 1.288×10^{-2})	(0.2124, 1.288×10^{-2})
(-0.5498 , 5.684×10^{-2})	(-0.5499 , 5.685×10^{-2})

TABLE 2. Flat plate. $M = 4.5$, $T_0 = 311$ K, $Pr = 0.72$, $Re = 1000$, $\omega = 0.2$, $\beta = 0.12$

eigenvalues, α , obtained with help of the RK solver at $\beta = 10^{-4}$ and results from Balakumar & Malik (1992) at $\beta = 0$. A comparison of eigenvalues α corresponding to $\beta = 0.12$ is given in table 2.

REFERENCES

- ASHPIS, D. & RESHOTKO, E. 1990 The vibrating ribbon problem revisited. *J. Fluid Mech.* **213**, 531–547.
- BALAKUMAR, P. & MALIK, M. R. 1992 Discrete modes and continuous spectra in supersonic boundary layer. *J. Fluid Mech.* **239**, 631–656.
- EGOROV, I. V., FEDOROV, A. V. & NECHAEV, A. V. 2004 Receptivity of supersonic boundary layer on a blunt plate to acoustic disturbances. *AIAA Paper* 2004-0249.
- EGOROV, I. V., FEDOROV, A. V. & SOUDAKOV, V. G. 2005 Direct numerical simulation of supersonic boundary layer receptivity to acoustic disturbances. *AIAA Paper* 2005-0097.
- EISLER, W. & BESTEK, H. 1993 Spatial numerical simulations of nonlinear transition phenomena in supersonic boundary layers. In *Transitional and Turbulent Compressible Flows* (ed. L. D. Kral & T. A. Zang). FED 151. ASME.
- FEDOROV, A. V. 1982 Generation and development of instability waves in a boundary layer of a compressible gas. PhD thesis, Moscow Institute of Physics and Technology (in Russian).
- FEDOROV, A. V. 1984 Excitation of Tollmien-Schlichting waves in a boundary layer by periodic external source located on the body surface. *Fluid Dyn.* **19**, 888–893.
- FEDOROV, A. V. 1988 Excitation of waves of instability of the secondary flow in the boundary layer on a swept wing. *J. Appl. Mech. Tech. Phys.* **29**, 643–648.
- FEDOROV, A. V. 2003a Receptivity of a high-speed boundary layer to acoustic disturbances. *J. Fluid Mech.* **491**, 101–129.
- FEDOROV, A. V. 2003b Receptivity of hypersonic boundary layer to acoustic disturbances scattered by surface roughness. *AIAA Paper* 2003-3731.
- FEDOROV, A. V. & KHOKHLOV, A. P. 1991 Mode switching in a supersonic boundary layer. *J. Appl. Mech. Tech. Phys.* **32**, 831–836.
- FEDOROV, A. V. & KHOKHLOV, A. P. 2001 Prehistory of instability in a hypersonic boundary layer. *Theor. Comp. Fluid Dyn.* **14**, 359–375.
- FEDOROV, A. V. & KHOKHLOV, A. P. 2002 Receptivity of hypersonic boundary layer to wall disturbances. *Theor. Comp. Fluid Dyn.* **15**, 231–254.
- FEDOROV, A. & TUMIN, A. 2003 Initial-value problem for hypersonic boundary layer flows. *AIAA J.* **41**, 379–389.
- FORGOSTON, E. & TUMIN, A. 2005 Initial-value problem for three-dimensional disturbances in a hypersonic boundary layer. *Phys. Fluids* **17**, 084106.
- GROSCH, C. E. & SALWEN, H. 1978 The continuous spectrum of the Orr–Sommerfeld equation. Part 1. the spectrum and eigenfunctions. *J. Fluid Mech.* **87**, 33–54.
- GUSHCHIN, V. R. & FEDOROV, A. V. 1989 Asymptotic analysis of inviscid perturbations in a supersonic boundary layer. *J. Appl. Mech. Tech. Phys.* **30**, 64–70.
- GUSTAVSSON, L. H. 1979 Initial-value problem for boundary layer flows. *Phys. Fluids* **22**, 1602–1605.
- GUYDOS, P. 2004 Analysis of small perturbations in compressible boundary layers. MS Thesis, The University of Arizona.
- GUYDOS, P. & TUMIN, A. 2004 Multimode decomposition in compressible boundary layers. *AIAA J.* **42**, 1115–1121.

- HANIFI, A., SCHMID, P. J. & HENNINGSON, D. S. 1996 Transient growth in compressible boundary layer flow. *Phys. Fluids* **8**, 826–837.
- HILL, D. C. 1995 Adjoint systems and their role in the receptivity problem for boundary-layers. *J. Fluid Mech.* **292**, 183–204.
- KAMKE, E. 1959 *Differentialgleichungen. Lösungsmethoden und Lösungen*. Leipzig: Akademische Verlagsgesellschaft Geest & Portig.
- MA, Y. & ZHONG, X. 2001 Numerical simulation of receptivity and stability of nonequilibrium reacting hypersonic boundary layers. *AIAA Paper* 2001-0892.
- MA, Y. & ZHONG, X. 2003a Receptivity of a supersonic boundary layer over a flat plate. Part 1: Wave structures and interactions. *J. Fluid Mech.* **488**, 31–78.
- MA, Y. & ZHONG, X. 2003b Receptivity of a supersonic boundary layer over a flat plate. Part 2: Receptivity to freestream sound. *J. Fluid Mech.* **488**, 79–121.
- MA, Y. & ZHONG, X. 2005 Receptivity of a supersonic boundary layer over a flat plate. Part 3: Effects of different types of free-stream disturbances. *J. Fluid Mech.* **532**, 63–109.
- MACK, L. M. 1969 Boundary layer stability theory. *JPL Report* 900-277. Jet Propulsion Lab., California Institute of Technology, Pasadena, CA, USA.
- MALIK, M. R. 1990 Numerical methods for hypersonic boundary layer stability. *J. Comput. Phys.* **86**, 376–413.
- NAYFEH, A. H. 1980 Stability of three-dimensional boundary layers. *AIAA J.* **18**, 406–416.
- SALWEN, H. & GROSCH, C. E. 1981 The continuous spectrum of the Orr–Sommerfeld equation. Part 2. Eigenfunction expansion. *J. Fluid Mech.* **104**, 445–465.
- SMITH, F. T., SYKES, R. I. & BRIGHTON, P. W. 1977 A two-dimensional boundary layer encountering a three-dimensional hump. *J. Fluid Mech.* **83**, 163–176.
- TERENT'EV, E. D. 1981 The linear problem of a vibrator in a subsonic boundary layer. *J. Appl. Math. Mech.* **45**, 791–795.
- TIKHONOV, A. N. & ARSEININ, V. Y. 1977 *Solutions of Ill-Posed Problems*. Wiley.
- TIKHONOV, A. N., GONCHARSKI, A. V., STEPANOV, V. V. & YAGOLA, A. G. 1995 *Numerical Methods for the Solution of Ill-Posed Problems*. Kluwer.
- TUMIN, A. 1983 Excitation of Tollmien–Schlichting waves in a boundary layer on a vibrating surface of an infinitely swept wing. *J. Appl. Mech. Tech. Phys.* **24**, 670–674.
- TUMIN, A. 1996 Receptivity of pipe Poiseuille flow. *J. Fluid Mech.* **315**, 119–137.
- TUMIN, A. 1998 Subharmonic resonance in a laminar wall jet. *Phys. Fluids* **10**, 1769–1771.
- TUMIN, A. 2003 Multimode decomposition of spatially growing perturbations in a two-dimensional boundary layer. *Phys. Fluids* **15**, 2525–2540.
- TUMIN, A. 2006a Biorthogonal eigenfunction system in the triple-deck limit. *Stud. Appl. Math.* **117**, 165–190.
- TUMIN, A. 2006b Receptivity of compressible boundary layers to three-dimensional wall perturbations. *AIAA Paper* 2006-1110.
- TUMIN, A. & AIZATULIN, L. 1997 Instability and receptivity of laminar wall jets. *Theor. Comp. Fluid Dyn.* **9**, 33–45.
- TUMIN, A., AMITAY, M., COHEN, J. & ZHOU, M. 1996 A normal multi-mode decomposition method for stability experiments. *Phys. Fluids* **8**, 2777–2779.
- TUMIN, A. M. & FEDOROV, A. V. 1983a Excitation of instability waves in a boundary layer on a vibrating surface. *J. Appl. Mech. Tech. Phys.* **24**, 670–674.
- TUMIN, A. M. & FEDOROV, A. V. 1983b Spatial growth of disturbances in a compressible boundary layer. *J. Appl. Mech. Tech. Phys.* **24**, 548–554.
- TUMIN, A. M. & FEDOROV, A. V. 1984 Excitation of instability waves by a vibrator localized in the boundary layer. *J. Appl. Mech. Tech. Phys.* **25**, 867–873.
- TUMIN, A. & RESHOTKO, E. 2003 Optimal disturbances in compressible boundary layers. *AIAA J.* **42**, 2357–2363.
- TUMIN, A. & RESHOTKO, E. 2004 The problem of boundary-layer flow encountering a three-dimensional hump revisited. *AIAA Paper* 2004-0101.
- TUMIN, A. & RESHOTKO, E. 2005 Receptivity of a boundary-layer flow to a three-dimensional hump at finite Reynolds numbers. *Phys. Fluids* **17**, 094101.
- TUMIN, A., WANG, X. & ZHONG, X. 2007 Direct numerical simulation and the theory of receptivity in a hypersonic boundary layer. *Phys. Fluids* **19**, 014101.

- WANG, X. & ZHONG, X. 2005 Receptivity of a Mach 8.0 flow over a sharp wedge with half-angle 5.3° to wall blowing-suction. *AIAA Paper* 2005-5025.
- WANG, X. & ZHONG, X. 2007 Numerical simulation of hypersonic boundary-layer receptivity to two and three-dimensional wall perturbations. *AIAA Paper* 2007-946.
- WOLFRAM, S. 1999 *The Mathematica Book*, 4th edn. Cambridge: Wolfram Media and Cambridge University Press.
- ZHIGULEV, V. N. & FEDOROV, A. V. 1987 Boundary layer receptivity to acoustic disturbances. *J. Appl. Mech. Tech. Phys.* **28**, 28–34.
- ZHIGULEV, V. N., SIDORENKO, N. V. & TUMIN, A. M. 1980 Generation of instability waves in a boundary layer by external turbulence. *J. Appl. Mech. Tech. Phys.* **21**, 774–778.
- ZHIGULEV, V. N. & TUMIN, A. M. 1987 *Origin of Turbulence*. Novosibirsk: Nauka (in Russian) [transl. NASA TT-20340, October 1988].
- ZHONG, X. & MA, Y. 2002 Receptivity and linear stability of Stetson's Mach 8 blunt cone stability experiments. *AIAA Paper* 2002-2849.